

# Head-on collisions of black holes: the particle limit

Carlos O. Lousto\* and Richard H. Price

*Department of Physics, University of Utah, Salt Lake City, UT 84112*

We compute gravitational radiation waveforms, spectra and energies for a point particle of mass  $m_0$  falling from rest at radius  $r_0$  into a Schwarzschild hole of mass  $M$ . This radiation is found to lowest order in  $(m_0/M)$  with the use of a Laplace transform. In contrast with numerical relativity results for head-on collisions of equal-mass holes, the radiated energy is found not to be a monotonically increasing function of initial separation; there is a local radiated-energy maximum at  $r_0 \approx 4.5M$ . The present results, along with results for infall from infinity, provide a complete catalog of waveforms and spectra for particle infall. We give a representative sample from that catalog and an interesting observation: Unlike the simple spectra for other head-on collisions (either of particle and hole, or of equal mass holes) the spectra for  $\infty > r_0 > \sim 5M$  show a series of evenly spaced bumps. A simple explanation is given for this. Lastly, our energy vs.  $r_0$  results are compared with approximation methods used elsewhere, for small and for large initial separation.

## I. INTRODUCTION AND OVERVIEW

Among the earliest calculations of astrophysical sources of gravitational radiation is the “DRPP” calculation [1] [2] of radiation emitted when a particle, starting from rest at infinity, falls into a nonspinning black hole. In this work, the mass of the particle is treated as a perturbation of the Schwarzschild spacetime and the Einstein equations, to first order in this perturbation, are organized into the Zerilli equation [3,4], a single linear wave equation. This work was later elaborated by Ruffini and Ferrari [5] who considered the head-on plunge of a particle which starts with nonzero inward velocity at spatial infinity.

There is now a renewed interest in such calculations. The advent of laser interferometric gravity wave detectors [6] has directed attention at black hole collisions as one of the most plausible, and surely the most fascinating, sources of detectable waves. But the generation of strong waves is a process without simplifying symmetries and one which involves strong field interactions. The challenge of finding energies and waveforms generated in these processes helped to spur the recent effort in numerical relativity and, in particular, in the Binary Black Hole supercomputing Grand Challenge [7]. Because of the difficulty of direct supercomputer solutions, approximate methods, as checks and guides, are very valuable. The “particle limit” in which the mass of one of the holes is very small, is in this category, and models of holes in binary orbits are a fundamental tool.

We are interested here in using a particle model to help in the understanding of numerical relativity results for collisions of holes. To date those computations have been limited to head on, axisymmetric collisions [8,9]. The codes have also been limited in the time for which they can evolve solutions. Infall from very large distances cannot at present be evolved; computations start from finite separation of the holes, so direct comparison with the DRPP results cannot be made. We present here an extension of the DRPP calculation to the case of infall from finite radius.

The extension is not at all straightforward. If the particle starts at infinity, the initial value data can be taken as zero, so that the spacetime is unperturbed Schwarzschild until the gravitational influence of the particle is felt. If the particle starts from finite radius, the specification of compatible initial value data cannot be avoided. Understanding the influence of the initial data is, in fact, a major motivation for the present work. Supercomputer evolution will be limited, for the foreseeable future, to evolving the interaction of holes for short times. The starting point for these evolutions will be initial data from some approximation method (e.g., a post-Newtonian expansion). The way to make the bridge from the approximation to the strong field realm of supercomputing requires that we understand what the crucial features are of the initial value data. It seems to us that the particle limit provides a very useful probe of this issue.

The remainder of the paper is organized as follows. In Sec. II we start by presenting the basic mathematical approach. Like the DRPP calculation, our approach uses frequency components. A Laplace transform converts the linearized Einstein equation for each  $\ell$ -pole, from a partial differential equation in Schwarzschild coordinates  $r, t$  to a

---

\*Electronic Address: lousto@mail.physics.utah.edu

set of ordinary differential equations in  $r$ . The Laplace transform treats the initial data mathematically as if it were a source, and helps with insight into the relation of the initial value data and the stress-energy source. Two points in particular should be noted in Sec. II. The first concerns the linearized wave equation. The equation presented by Zerilli was formulated in the Regge-Wheeler gauge [10], a specific first order coordinate choice. The Zerilli equation was presented through a Fourier transform and has no direct equivalent as a partial differential equation. This is not a fundamental obstacle, but it does complicate the relationship of the Zerilli wave function and the initial data. To avoid these problems we use the Moncrief formulation of the problem [4]. Moncrief's wave function is constructed explicitly from initial data and is equivalent to the Zerilli wave function except for source-like terms. The second point to notice has to do with conventions. A variety of conventions has been used for normalizing the Zerilli (or Moncrief) functions and their transforms. In Sec. II, we present a definition of all our conventions and their relationship to those used elsewhere.

Aspects of the numerical approach, a Green function integral, are discussed in Sec. III. A major issue is the need for highly accurate evaluation of the Green function integrals in order to preclude numerical errors from giving rise to an erroneous initial burst of radiation. Numerical results are presented in Sec. IV for energy, spectra, and waveforms. Plots are given for infall starting from rest at radii ranging from  $r_0/2M = 1.1$  to  $r_0/2M = 15$ . These are combined with results for infall from infinity to give a complete picture of the dependence of the radiation on the initial physical conditions. The numerical results are discussed in Sec. V and are compared with predictions based on other results and approximations, especially those of the close-limit approximation.

Throughout the rest of the paper we use  $c = G = 1$  units, the signature  $-+++$ , and other conventions of the Misner, Thorne and Wheeler textbook [11].

## II. MATHEMATICAL APPROACH

### A. Variables and conventions

For the straight-line plunge of a particle into a nonspinning hole the perturbations of the Schwarzschild spacetime are all even-parity. We take the particle to be moving along the  $z$  axis, so that the perturbations are not dependent on the azimuthal angle  $\phi$ . To describe the perturbations we use the notation of Regge and Wheeler [10], here specialized to the axisymmetric  $\ell$ -pole case ( $m = 0$ ):

$$\begin{aligned} ds^2 = & ds_0^2 + (1 - 2M/r)(H_0 Y_{\ell 0}) dt^2 + (1 - 2M/r)^{-1} (H_2 Y_{\ell 0}) dr^2 \\ & + r^2 (K Y_{\ell 0} + G \partial^2 Y_{\ell 0} / \partial \theta^2) d\theta^2 + r^2 (\sin^2 \theta K Y_{\ell 0} + G \sin \theta \cos \theta \partial Y_{\ell 0} / \partial \theta) d\phi^2 \\ & + 2H_1 Y_{\ell 0} dt dr + 2h_0 (\partial Y_{\ell 0} / \partial \theta) dt d\theta + 2h_1 (\partial Y_{\ell 0} / \partial \theta) dr d\theta \end{aligned} \quad (2.1)$$

where  $ds_0^2$  is the unperturbed line element for a Schwarzschild spacetime of mass  $M$ , where  $H_0, H_1, H_2, h_0, h_1, K$  and  $G$  are functions of  $r, t$ , and where  $Y_{\ell 0}(\theta)$  are the  $m = 0$  spherical harmonics. We then follow the prescription given by Moncrief [4] in his eqs. (5.8) – (5.12) and (5.27) to arrive at a wave function. Rather than choose the normalization of Moncrief's "Q" we choose a normalization closely related to Zerilli's [3] wave function. In the Regge-Wheeler [10] gauge ( $G = h_0 = h_1 = 0$ ) this "Moncrief-Zerilli" function is

$$\psi(r, t) = \frac{r}{\lambda + 1} \left[ K + \frac{r - 2M}{\lambda r + 3M} \{ H_2 - r \partial K / \partial r \} \right] \quad (2.2)$$

where we have used Zerilli's notation

$$\lambda \equiv (\ell + 2)(\ell - 1)/2. \quad (2.3)$$

We now give the relationship of this variable, which we shall use throughout the paper, to the following wavefunctions: (i)  $Q$  appearing in Moncrief's [4] eq. (5.27) (ii)  $\psi_{\text{pert}}$  and  $\psi_{\text{num}}$  appearing in Ref. [12]. For  $\ell = 2$  the wave function appearing as  $\tilde{\psi}$  in eq. (II-31) of Cunningham, Price and Moncrief [13], and  $\psi$  defined in eq. (13) of Price and Pullin [14], agree with  $\psi_{\text{pert}}$ . The relations are:

$$\begin{aligned} \psi &= 2Q / [\ell(\ell + 1)] \\ &= 2[(\ell - 2)! / (\ell + 2)!] \psi_{\text{pert}} \\ &= \sqrt{2[(\ell - 2)! / (\ell + 2)!]} \psi_{\text{num}}. \end{aligned} \quad (2.4)$$

Zerilli [3] derives his equation only in the frequency domain, so no direct comparison can be made with functions of  $r, t$ . It is, however, straightforward to use the same steps as Zerilli in the Regge-Wheeler gauge. but confined to the  $r, t$  domain. It turns out that to decouple the even-parity variables in the perturbed Einstein equations, one needs to take an extra time derivative. One can then define the variable  $\psi_{\text{Zer}}(r, t)$  by

$$\dot{\psi}_{\text{Zer}} = \frac{r^2 \dot{K} - (r - 2M)H_1}{\lambda r + 3M}, \quad (2.5)$$

where the dot indicates a derivative with respect to  $t$ . The Fourier transform of this variable, divided by  $-i\omega$  is the function defined in Zerilli's papers. For vacuum perturbations  $\dot{\psi}_{\text{Zer}} = \dot{\psi}$ , so the Zerilli wave function, in vacuum, can be chosen to agree with our  $\psi$ .

By computing the stress-energy pseudotensor in a radiation gauge, we find that radiated power per solid angle is

$$\frac{d\text{Power}}{d\Omega} = \frac{1}{64\pi} \left[ \frac{\partial\psi}{\partial u} \right]^2 \left( \cot\theta \frac{\partial}{\partial\theta} Y_{\ell 0} - \frac{\partial^2}{\partial\theta^2} Y_{\ell 0} \right)^2 \quad (2.6)$$

(where  $u$  is retarded time), so that the gravitational wave power, integrated over all angles, is

$$\text{Power} = \frac{1}{64\pi} \frac{(\ell + 2)!}{(\ell - 2)!} \left[ \frac{\partial\psi}{\partial u} \right]^2. \quad (2.7)$$

Our wave function  $\psi$  satisfies a second-order wave equation with a source term,

$$-\frac{\partial^2\psi}{\partial t^2} + \frac{\partial^2\psi}{\partial r^{*2}} - V_\ell(r)\psi = \mathcal{S}_\ell(r, t). \quad (2.8)$$

Here  $r^* \equiv r + 2M \ln(r/2M - 1)$  is the Regge-Wheeler [10] ‘‘tortoise’’ coordinate,  $V_\ell$  is the Zerilli potential

$$V_\ell(r) = \left( 1 - \frac{2M}{r} \right) \frac{2\lambda^2(\lambda + 1)r^3 + 6\lambda^2 Mr^2 + 18\lambda M^2 r + 18M^3}{r^3(\lambda r + 3M)^2}, \quad (2.9)$$

and  $\mathcal{S}_\ell(r, t)$  is the source term.

We are interested in the case in which the source is a point particle, of mass  $m_0$ , following a spacetime trajectory given by  $t = T(\tau)$ , and  $r = R(\tau)$ , where  $\tau$  is proper time along the particle world line,

$$T^{\mu\nu} = (m_0/U^0)U^\mu U^\nu \delta(r - R)\delta^2(\Omega)/r^2. \quad (2.10)$$

Here  $U^\mu \equiv dx^\mu/d\tau$  is the particle 4-velocity, and the 0-component is  $U^0 = \varepsilon_0/(1 - 2M/r)$ , where  $\varepsilon_0 = -U_0$ , the ‘‘energy-at-infinity per unit particle mass,’’ is a constant of motion that takes the value  $\sqrt{1 - 2M/r_0}$  for infall from rest at  $r_0$ . The two dimensional delta function  $\delta^2(\Omega)$  gives the angular location of the particle trajectory

$$\delta^2(\Omega) = \sum_{\ell, m} Y_{\ell m}(\theta, \phi) Y_{\ell m}^*(\theta, \phi) = \sum_{\ell} Y_{\ell 0}(\theta) \sqrt{(2\ell + 1)/4\pi}, \quad (2.11)$$

with the last expression applying for infall along the positive  $z$  axis.

We now need to write the the Einstein ( $G_{\mu\nu}$ ) and Ricci ( $R_{\mu\nu}$ ) tensors, in a tensor spherical harmonic decomposition like that in (2.1). The components we shall need are:

$$G_{00} \equiv \sum_{\ell} G44 Y_{\ell 0} \quad R_{00} \equiv \sum_{\ell} R44 Y_{\ell 0} \quad R_{\theta\theta} \equiv \sum_{\ell} (R22K Y_{\ell 0} + R22G \partial^2 Y_{\ell 0} / \partial\theta^2). \quad (2.12)$$

(Here, and below, we omit  $\ell$  indices where the meaning of the symbols – such as  $G44$  – is clear from context.) By rearranging the expressions for the perturbed Einstein and Ricci components, we find that the source term in (2.8), for an axisymmetric problem, is

$$\mathcal{S}_\ell(r, t) = \frac{2(1 - 2M/r)}{r(\lambda + 1)(\lambda r + 3M)} \left[ r^2 \left( 1 - \frac{2M}{r} \right) \frac{\partial}{\partial r} R22K - (\lambda r + M) R22K - \frac{r^4 \lambda}{\lambda r + 3M} G44 + r^3 R44 \right]. \quad (2.13)$$

The Einstein equations can now be used to replace the perturbed Ricci and Einstein components with components of the particle stress energy

$$\begin{aligned} G_{44} &= \kappa U^0 (1 - 2M/r)^2 \delta(r - R) / r^2 \\ R_{44} &= \kappa \left[ (1 - 2M/r)^2 U^0 - \frac{1}{2U^0} (1 - 2M/r) \right] \delta(r - R) / r^2 \\ R_{22} K &= \kappa \left[ \delta(r - R) / 2U^0 \right] , \end{aligned} \quad (2.14)$$

where

$$\kappa \equiv 8\pi m_0 \sqrt{(2\ell + 1) / 4\pi} . \quad (2.15)$$

When these are used in (2.13) the result is

$$\begin{aligned} \mathcal{S}_\ell(r, t) &= -\frac{2(1 - 2M/r)\kappa}{r(\lambda + 1)(\lambda r + 3M)} \left[ -r^2 (1 - 2M/r) \frac{1}{2U^0} \delta'(r - R) \right. \\ &\quad \left. + \left\{ \frac{r(\lambda + 1) - M}{2U^0} - \frac{3MU^0 r (1 - 2M/r)^2}{r\lambda + 3M} \right\} \delta(r - R) \right] . \end{aligned} \quad (2.16)$$

When the source term is included, the relation between our wave function  $\psi$ , and the Zerilli wave function of (2.5) becomes

$$\dot{\psi} = \dot{\psi}_{\text{Zer}} - \frac{\kappa U^0 (r - 2M)}{(\lambda + 1)(\lambda r + 3M)} \frac{dR}{dt} \delta(r - R) . \quad (2.17)$$

## B. Initial data

For comparison with established results of numerical relativity we want initial data representing an initially stationary spacetime, so we take  $\dot{\psi}_0$ , the initial time derivative of  $\psi$ , to be zero. To determine our  $\psi_0$ , the initial value of  $\psi$ , we choose an initial 3-geometry with the conformally flat form that is used in numerical relativity [15,16],

$$ds^2 = \Phi(\bar{r}, \theta)^4 [d\bar{r}^2 + \bar{r}^2(d\theta^2 + \sin^2 \theta d\phi^2)] , \quad (2.18)$$

where  $\Phi$  satisfies a flat-space Laplace equation  $\nabla^2 \Phi = 0$ . We choose  $\Phi$  to represent a throat of mass  $m_1$  on the  $z$  axis at  $z = z_1$  and a throat of mass  $m_2$  at  $z = z_2$ . The simplest such solution has the form

$$\Phi = 1 + \frac{1}{2} \left( \frac{m_1}{\sqrt{\bar{r}^2 \sin^2 \theta + (\bar{r} \cos \theta - z_1)^2}} + \frac{m_2}{\sqrt{\bar{r}^2 \sin^2 \theta + (\bar{r} \cos \theta - z_2)^2}} \right) . \quad (2.19)$$

We now identify  $M \equiv m_1 + m_2$ , and choose  $z_1 = -z_2(m_2/m_1)$  so that the dipole moment vanishes for  $\bar{r} > z_2$ . We treat the mass ratio  $m_2/M$  as small and keep terms in (2.19) only to first order in this ratio. We ignore the nonradiative  $\ell = 0, 1$  perturbations and write  $\Phi$  as

$$\Phi = 1 + \frac{M}{2\bar{r}} + \frac{m_2}{2\bar{r}} \sum_{\ell=2,3,\dots} \mathcal{F}_\ell(\bar{r}) P_\ell(\cos \theta) \quad (2.20)$$

where

$$\mathcal{F}_\ell(\bar{r}) = \begin{cases} (z_2/\bar{r})^\ell & \text{if } \bar{r} > z_2 \\ (\bar{r}/z_2)^{\ell+1} & \text{if } \bar{r} < z_2 \end{cases} . \quad (2.21)$$

We next change radial variables, from isotropic-like  $\bar{r}$  to a Schwarzschild-like coordinate  $r$ , with the transformation

$$\bar{r} = \left( \sqrt{r} + \sqrt{r - 2M} \right)^2 / 4 . \quad (2.22)$$

When this is used in (2.18), and terms higher order in  $m_2$  are omitted, the result is

$$ds^2 = \left( 1 + \frac{2m_2/\bar{r}}{1 + M/2\bar{r}} \sum_{\ell=2,3,\dots} \mathcal{F}_\ell(\bar{r}) P_\ell(\cos\theta) \right) \left[ \frac{dr^2}{1 - 2M/r} + r^2(d\theta^2 + \sin^2\theta d\phi^2) \right]. \quad (2.23)$$

From this we can infer that the initial value perturbations in the Regge-Wheeler notation of (2.1) are  $G = h_1 = 0$  and

$$K = H_2 = \frac{2m_2/\bar{r}}{1 + M/2\bar{r}} \mathcal{F}_\ell(\bar{r}) \sqrt{\frac{4\pi}{2\ell + 1}}. \quad (2.24)$$

We must now complete the identification of this conformally flat solution with the point particle solution. Clearly the location  $\bar{r} = z_2$  of the perturbative throat must be set to

$$z_2 \equiv \bar{r}_0 = \left( \sqrt{r_0} + \sqrt{r_0 - 2M} \right)^2 / 4. \quad (2.25)$$

The mass  $m_2$  of the throat must *not* be set to the mass  $m_0$  of the particle. The particle mass  $m_0$  can be viewed as the “bare” mass of the particle, the mass that is measured very close to the location of the particle. On the other hand,  $m_2$  is a formal parameter of the initial value solution; since the total ADM mass for (2.19) is  $m_1 + m_2$ , gravitational binding energy is included in  $m_2$ . We give here two arguments for the correct relationship. The first is based on the definition, given by Brill and Lindquist [15], of “bare” mass for a solution with the form (2.19), a mass exclusive of binding energy. To find an expression for this bare mass they look at the extension of the geometry through the perturbative throat into an asymptotically flat universe; the bare mass of the perturbative throat is the mass measured at infinity in that universe. From eq. (13) of Ref. [15] the bare mass of the perturbative throat (to first order in  $m_2/M$ ) is

$$m_2^{\text{bare}} = m_2(1 + M/2\bar{r}_0). \quad (2.26)$$

We identify the bare mass with the particle mass  $m_0$  and conclude

$$m_2 = m_0 \left( 1 + \frac{M}{2\bar{r}_0} \right)^{-1} = \frac{1}{2} m_0 \left( 1 + \sqrt{1 - \frac{2M}{r_0}} \right). \quad (2.27)$$

An independent way of finding the relationship is to look at the perturbed hamiltonian constraint. For a conformally flat ( $H_0 = H_2 = K$ ) initial 3-geometry [equivalent to eq. (C7a) of Ref. [17]] this gives us

$$\begin{aligned} \left( 1 - \frac{2M}{r} \right)^2 \frac{\partial^2 K}{\partial r^2} + \left( 1 - \frac{2M}{r} \right) \left( 2 - \frac{3M}{r} \right) \frac{1}{r} \frac{\partial K}{\partial r} - \left( 1 - \frac{2M}{r} \right) \frac{\ell(\ell + 1)}{r^2} K &= -G_{44} \\ &= -8\pi m_0 \sqrt{\frac{2\ell + 1}{4\pi}} U^0 \left( 1 - \frac{2M}{r} \right)^2 \frac{1}{r^2} \delta(r - r_0). \end{aligned} \quad (2.28)$$

By integrating across the discontinuity, and by using (2.21), (2.22), and (2.24), we find

$$\begin{aligned} \Delta K_{,r} &\equiv dK/dr|_{r=r_0^+} - dK/dr|_{r=r_0^-} \\ &= -8\pi m_2 \frac{\sqrt{(2\ell + 1)/4\pi}}{\bar{r}_0^{1/2} r_0^{3/2} \sqrt{1 - 2M/r_0}} \\ &= -8\pi m_0 \frac{\sqrt{(2\ell + 1)/4\pi}}{r_0^2 \sqrt{1 - 2M/r_0}}, \end{aligned} \quad (2.29)$$

which gives us the same relationship as in (2.27). This second derivation of the mass relationship is instructive. If we choose a conformally flat initial geometry then all the information about the perturbations of that geometry is contained in the single function  $K(r)$ . But (2.28) completely fixes  $K(r)$ , so the initial geometry has no freedom. (Alternatively: To choose different initial data we would have to introduce nonconformally-flat terms.) This is to be contrasted with the case of nonperturbative throats, where a variety of choices is possible for conformally flat initial data.

### C. Laplace transforms

We now define the Laplace transform  $\Psi$  of  $\psi$  to be

$$\Psi(r, \omega) \equiv \int_0^\infty e^{i\omega t} \psi(r, t) dt . \quad (2.30)$$

We take  $\psi$  to vanish for  $t < 0$ , which means that  $\Psi(r, \omega)$  must be analytic in the upper half of the complex  $\omega$  plane. At large  $r$ , for outgoing waves,  $\psi(r, t)$  is a function only of  $t - r^*$  so  $\Psi$  takes the form

$$\Psi(r, \omega) \rightarrow A(\omega) e^{i\omega r^*} . \quad (2.31)$$

We call  $A$  the amplitude of the outgoing radiation. Since the outgoing radiation  $\psi(r, t)$  is pure real, the amplitude satisfies the crossing relation  $A(-\omega) = A^*(\omega)$ .

The waveform for outgoing radiation, as a function of retarded time  $u \equiv t - r^*$  can be found by the inverse transform

$$\psi(u) = \frac{1}{2\pi} \int_{-\infty}^{+\infty} A(\omega) e^{-i\omega u} d\omega = \text{Re} \left[ \frac{1}{\pi} \int_0^\infty A(\omega) e^{-i\omega u} d\omega \right] . \quad (2.32)$$

For a particle falling in from infinity the waveform extends to  $u \rightarrow -\infty$ , and there is no initial data to deal with. In this case  $A(\omega)$  is to be interpreted as a Fourier, rather than Laplace, transform. If the particle has  $\varepsilon_0 > 1$ , then the waveform does not vanish at  $u \rightarrow -\infty$ , and the transform exists only for  $\omega$  in the lower half plane, and will have a pole at  $\omega = 0$ . For the inverse transform (the first integral in (2.32) the contour should be interpreted as going below the real  $\omega$  axis, so the integral is the equivalent of the Cauchy principal value plus half the contribution of the residue of the pole at  $\omega = 0$ ,

$$\psi(u) = \text{Re} \left[ \lim_{\epsilon \rightarrow 0} \frac{1}{\pi} \int_\epsilon^\infty A(\omega) e^{-i\omega u} d\omega \right] + \frac{i}{2} \lim_{\omega \rightarrow 0} \{\omega A(\omega)\} . \quad (2.33)$$

From Parseval's theorem and (2.7), we have that the radiated energy at Scri+ is

$$\begin{aligned} \text{Energy} &= \frac{1}{64\pi} \frac{(\ell+2)!}{(\ell-2)!} \int_{-\infty}^\infty \left( \frac{d\psi}{du} \right)^2 dt \\ &= \frac{1}{128\pi^2} \frac{(\ell+2)!}{(\ell-2)!} \int_{-\infty}^\infty \omega^2 |A(\omega)|^2 d\omega \\ &= \frac{1}{64\pi^2} \frac{(\ell+2)!}{(\ell-2)!} \int_0^\infty \omega^2 |A(\omega)|^2 d\omega . \end{aligned} \quad (2.34)$$

The energy spectrum is therefore given by

$$\frac{d\text{Energy}}{d\omega} = \frac{1}{64\pi^2} \frac{(\ell+2)!}{(\ell-2)!} \omega^2 |A(\omega)|^2 . \quad (2.35)$$

We now multiply (2.8) by  $e^{i\omega t}$ , integrate from  $t = 0$  to  $\infty$ , and integrate by parts in the integral involving  $\partial^2 \psi / \partial t^2$ . The result is an ordinary differential equation for  $\Psi$ :

$$\frac{\partial^2 \Psi}{\partial r_*^2} + [\omega^2 - V_\ell(r)] \Psi = -\dot{\psi}_0(r) + i\omega \psi_0(r) + S(r, \omega) , \quad (2.36)$$

where  $\psi_0(r)$  is the initial value of  $\psi(t, r)$ , and  $\dot{\psi}_0(r)$  is the initial value of  $\dot{\psi}(t, r)$ , and the source term  $S$  is defined as

$$S(r, \omega) \equiv \int_0^\infty e^{i\omega t} \mathcal{S}_\ell(r, t) dt . \quad (2.37)$$

For the particle source we substitute (2.16) into (2.37), to get

$$\begin{aligned} S(r, \omega) &= \frac{2(1-2M/r)\kappa}{r(\lambda+1)(\lambda r+3M)} \left[ -r^2(1-2M/r) \left\{ \frac{1}{|\dot{R}|} \frac{d}{dt} \left( \frac{e^{i\omega t}}{2U^0 \dot{R}} \right) \right\} \right. \\ &\quad \left. + \frac{1}{|\dot{R}|} \left\{ \frac{r(\lambda+1)-M}{2U^0} - \frac{3MU^0 r(1-2M/r)^2}{r\lambda+3M} \right\} e^{i\omega t} \right]_{T(r)} . \end{aligned} \quad (2.38)$$

The subscript “ $T(r)$ ” indicates that functions of time, such as  $\dot{R} \equiv dR/dt, U^0, e^{i\omega t}$  are to be evaluated at the value of  $t = T(r)$  where  $T = T(\tau)$  with  $r = R(\tau)$ . For infall from rest at radius  $r_0$ , this gives  $t$  as a function of  $r$  through

$$\begin{aligned} T(r) = & \varepsilon_0 \left( \frac{r_0}{2M} \right) \left( \frac{r}{2M} \right)^{1/2} \sqrt{1 - \frac{r}{r_0}} \\ & + \left( 1 + \frac{4M}{r_0} \right) \left( \frac{r_0}{2M} \right)^{3/2} \varepsilon_0 \arctan \left[ \sqrt{\frac{r_0}{r} - 1} \right] \\ & + 2 \operatorname{arctanh} \left[ \varepsilon_0^{-1} \sqrt{\frac{2M}{r} - \frac{2M}{r_0}} \right]. \end{aligned} \quad (2.39)$$

The result in (2.38) for  $S(r, \omega)$ , however, is not valid for  $r = r_0$ . When  $r = r_0$  the delta functions in (2.16), as functions of  $t$ , have vanishing arguments at  $t = 0$ , the endpoint of  $t$  integration in (2.37), so the integration is not well defined. The way to deal with this will be explained in the next section.

### III. COMPUTATIONAL IMPLEMENTATION

#### A. Green function formal solution

We start by rewriting (2.36) in the form

$$\frac{\partial^2 \Psi}{\partial r^{*2}} + [\omega^2 - V_\ell(r)] \Psi = S_{\text{tot}}(r, \omega), \quad (3.1)$$

where  $S_{\text{tot}}$  is the complete right hand side of (2.36), including both the stress energy term and the initial value terms,

$$S_{\text{tot}}(\omega, r) = -\dot{\psi}_0(r) + i\omega\psi_0(r) + S(r, \omega). \quad (3.2)$$

This equation is to be solved for the boundary conditions of ingoing waves at the horizon, and outgoing waves at spatial infinity:  $\Psi \rightarrow e^{-i\omega r^*}$  for  $r^* \rightarrow -\infty$ , and  $\Psi \rightarrow e^{i\omega r^*}$  for  $r^* \rightarrow +\infty$ . The Green function solution is found in the usual way. We define  $y_L(r^*, \omega)$  and  $y_R(r^*, \omega)$  as the homogeneous solutions of (3.1) with asymptotic forms

$$\begin{aligned} y_L(r^*, \omega) & \xrightarrow{r^* \rightarrow -\infty} e^{-i\omega r^*} \\ y_R(r^*, \omega) & \xrightarrow{r^* \rightarrow \infty} e^{i\omega r^*}. \end{aligned} \quad (3.3)$$

We define the Wronskian of the homogeneous solutions, an  $r^*$ -independent constant, to be

$$W(\omega) \equiv y_L \frac{d}{dr^*} y_R - y_R \frac{d}{dr^*} y_L. \quad (3.4)$$

With the above definitions, the Green function solution is written

$$\Psi(r, \omega) = \frac{1}{W(\omega)} \left[ y_R(r^*, \omega) \int_{-\infty}^{r^*} S_{\text{tot}}(\tilde{r}, \omega) y_L(\tilde{r}^*, \omega) d\tilde{r}^* + y_L(r^*, \omega) \int_{r^*}^{\infty} S_{\text{tot}}(\tilde{r}, \omega) y_R(\tilde{r}^*, \omega) d\tilde{r}^* \right]. \quad (3.5)$$

In the limit of large  $r^*$  this gives us

$$A(\omega) = \frac{1}{W(\omega)} \int_{-\infty}^{\infty} S_{\text{tot}}(r, \omega) y_L(r^*, \omega) dr^*. \quad (3.6)$$

## B. Evaluation of the Green function integral

The first two terms in (3.2) are straightforward to integrate in (3.6), but the stress energy source term  $S(r, \omega)$  cannot be evaluated at  $r_0$ . [The expression in (2.38) formally diverges as  $(r - r_0)^{-3/2}$  and hence cannot be used in (3.6).] To make sense of this we start by writing the source in (2.16) as

$$S(r, t) = F(r, t)\delta'(r - R[t]) + G(r, t)\delta(r - R[t]) , \quad (3.7)$$

where  $F$  and  $G$  contain no delta functions. The troublesome part of the Green function integral can then be written as

$$\int_{-\infty}^{+\infty} S(r, \omega)y_L(r^*, \omega) dr^* = \mathcal{I}_1 + \mathcal{I}_2 , \quad (3.8)$$

where  $\mathcal{I}_1$  is the integral involving  $G$  and  $\mathcal{I}_2$  involves  $F$ . The first of these is

$$\begin{aligned} \mathcal{I}_1 &= \int_0^{+\infty} e^{i\omega t} dt \int_{-\infty}^{\infty} y_L(r^*, \omega) dr^* G(r, t)\delta(r - R) \\ &= \int_0^{\infty} e^{i\omega t} dt \int_{2M}^{\infty} y_L(r^*, \omega) G(r, t)\delta(r - R) \frac{dr}{1 - 2M/r} \\ &= \int_0^{\infty} e^{i\omega t} y_L(r^*(t), \omega) G(R(t), t) dt / (1 - 2M/R(t)) \\ &= - \int_{-\infty}^{r_0^*} e^{i\omega T(r)} y_L(r^*, \omega) G(r, T(r)) dr^* / \dot{R} . \end{aligned} \quad (3.9)$$

In the final integral, the factor  $1/\dot{R} \sim (r - r_0)^{-1/2}$  diverges but is integrable. A similar set of transformations is now applied to  $\mathcal{I}_2$ ,

$$\begin{aligned} \mathcal{I}_2 &= \int_0^{+\infty} e^{i\omega t} dt \int_{-\infty}^{\infty} y_L(r^*, \omega) F(r, t)\delta'(r - R) dr^* \\ &= \int_0^{\infty} e^{i\omega t} dt \int_{2M}^{\infty} y_L(r^*, \omega) F(r, t)\delta'(r - R) \frac{dr}{1 - 2M/r} \\ &= - \int_0^{\infty} e^{i\omega t} dt \left[ y_L(r^*(t), \omega) \frac{\partial}{\partial r} \left( \frac{F}{1 - 2M/r} \right) + \frac{F}{(1 - 2M/r)^2} \frac{\partial}{\partial r^*} (y_L(r^*(t), \omega)) \right]_{r=R(t)} \\ &= \int_{-\infty}^{r_0^*} e^{i\omega T(r)} \left[ \left( 1 - \frac{2M}{r} \right) \frac{\partial}{\partial r} \left( \frac{F}{1 - 2M/r} \right) y_L(r^*, \omega) + \left( \frac{F}{1 - 2M/r} \right) \frac{\partial}{\partial r} (y_L(r^*, \omega)) \right] \frac{dr^*}{\dot{R}} . \end{aligned} \quad (3.10)$$

To evaluate these explicitly we need the fact that for free fall from rest at  $r_0$

$$\dot{R} = - \left( 1 - \frac{2M}{r} \right) \sqrt{\frac{2M/r - 2M/r_0}{1 - 2M/r_0}} . \quad (3.11)$$

We can now use the explicit expressions for  $F(r, t), G(r, t)$  from (2.16) to write

$$\begin{aligned} \mathcal{I}_1 + \mathcal{I}_2 &= - \frac{\kappa}{\lambda + 1} \int_{-\infty}^{r_0^*} \frac{e^{i\omega T(r)} dr^*}{\sqrt{2M/r - 2M/r_0}} \frac{(1 - 2M/r)}{(\lambda r + 3M)} \left[ r \frac{\partial}{\partial r^*} y_L \right. \\ &\quad \left. + y_L \left\{ \lambda + 1 - \frac{M}{r} + \frac{(2\lambda - 3 + 12M/r_0)M}{\lambda r + 3M} \right\} \right] . \end{aligned} \quad (3.12)$$

From (3.6), (3.2), and the definitions of  $\mathcal{I}_1 + \mathcal{I}_2$ , we have that

$$A(\omega) = \frac{1}{W(\omega)} \left[ \mathcal{I}_1 + \mathcal{I}_2 + i\omega \int_{-\infty}^{\infty} \psi_0(r) y_L(r^*, \omega) dr^* - \int_{-\infty}^{\infty} \dot{\psi}_0(r) y_L(r^*, \omega) dr^* \right] . \quad (3.13)$$

Since we are considering an initially stationary problem we have  $\dot{\psi}_0 = 0$ . The initial data for  $\psi$  comes from putting (2.24) in (2.2):

$$\psi_0 = \frac{2m_2}{\lambda+1} \frac{\sqrt{4\pi/(2\ell+1)}}{1+M/2\bar{r}} \frac{r}{\lambda r+3M} \times \left[ \left( (\lambda+1)r + M - r\sqrt{1-2M/r} \frac{M/2\bar{r}}{1+M/2\bar{r}} \right) \left\{ \frac{\bar{r}_0^\ell/\bar{r}^{\ell+1}}{\bar{r}^\ell/\bar{r}_0^{\ell+1}} \right\} - r\sqrt{1-\frac{2M}{r}\bar{r}} \left\{ \frac{-(\ell+1)\bar{r}_0^\ell/\bar{r}^{\ell+2}}{\ell\bar{r}^{\ell-1}/\bar{r}_0^{\ell+1}} \right\} \right], \quad (3.14)$$

where the upper expressions apply in the case  $\bar{r} > \bar{r}_0$ , and the lower for  $\bar{r} < \bar{r}_0$ .

It should be noted that  $\psi_0$  approaches a nonzero constant, and  $y_L(r^*, \omega) \rightarrow e^{-i\omega r^*}$ , as  $r \rightarrow 2M$ , so the integral over  $\psi_0$ , in (3.13) is improper at large negative  $r^*$ . We must recall that we are really computing  $A$  in the upper half of the complex  $\omega$  plane. To deal with this computationally we recast the integral in (3.13) into the form

$$\int_{-\infty}^{\infty} \psi_0(r) y_L(r^*, \omega) dr^* \rightarrow i\omega^{-1} \psi_0(2M) e^{-i\omega r_{\text{start}}^*} + \int_{r_{\text{start}}^*}^{\infty} \psi_0(r) y_L(r^*, \omega) dr^*. \quad (3.15)$$

where  $\psi_0(2M)$  is the limit of  $\psi_0$  at  $r = 2M$ . The value of  $r_{\text{start}}^*$  must be chosen such that there is negligible variation of  $\psi$  between  $r_{\text{start}}^*$  and the horizon.

### C. Numerical method

The first step in the solution is to determine the Wronskian in (3.4). We denote the form of  $y_L$  at large  $r$  by

$$y_L \xrightarrow{r \rightarrow \infty} \alpha(\omega) e^{i\omega r^*} + \beta(\omega) e^{-i\omega r^*}. \quad (3.16)$$

We find  $\beta(\omega)$  by solving (3.1) with the righthand side set to zero, and with the starting condition  $y_L = e^{-i\omega r^*}$  imposed at a large negative value of  $r^*$ . A fourth-order Runge-Kutta routine is used to integrate  $y_L$  out to large values of  $r^*$  where it is matched to approximate forms of the asymptotic solution. In practice, good accuracy was difficult to achieve with the asymptotic form in (3.16) and asymptotic solutions one order higher in  $1/\omega r$  were used. From  $\beta$ , the Wronskian follows immediately:

$$W(\omega) = 2i\omega\beta(\omega). \quad (3.17)$$

With  $\beta$  in hand, with  $\dot{\psi}_0 = 0$ , and with the substitution in (3.15), the problem consists of computing

$$A(\omega) = \frac{1}{2i\omega\beta(\omega)} \left[ \mathcal{I}_1 + \mathcal{I}_2 - \psi_0(2M) e^{-i\omega r_{\text{start}}^*} + i\omega \int_{r_{\text{start}}^*}^{\infty} \psi_0(r) y_L(r^*, \omega) dr^* \right], \quad (3.18)$$

where  $\mathcal{I}_1 + \mathcal{I}_2$  is the integral given in (3.12) and  $\psi_0$  is given in (3.14). A numerical solution for  $A(\omega)$  is found by using a fourth-order Runge-Kutta routine to solve for  $y_L$  and  $dy_L/dr^*$ , and the integral in (3.18) is done by Simpson's rule. From the solution for  $A$  the energy spectrum is computed with (2.35), and the waveform from (2.32).

The numerical solution used a routine to find the ‘‘particle contribution,’’  $\mathcal{I}_1 + \mathcal{I}_2$ , and one for the ‘‘initial value contribution,’’ the integral over  $\psi_0$  in (3.18). For both routines, second-order convergence was found and Richardson extrapolation was used. The step size in the Runge-Kutta and integration routines were halved until the Richardson extrapolate agreed with that from the next larger grid within a preset error limit. The initial value contribution could be usually be found within an error of 0.2%, while the particle contributions required an error preset of 0.5%. For most values of  $\ell, \omega, r_0$ , these precision requirements were easily met. The exception was a relatively small number of points at which the real and imaginary parts of a contribution differed by more than an order of magnitude. In this case it was difficult to get high accuracy in the smaller part.

An estimate of the error in our results is complicated by the fact that the physically important results are a superposition of the particle and initial value contributions, and significant cancellations occur in this superposition. These cancellations, in principle, mean that the error may be much larger than the small relative error in each contribution. To arrive at an estimate of the error in our determinations of the radiated energy we have recomputed the energy for four trials, in which  $\pm 0.5\%$  was added to the particle contribution, and then to the initial value contribution. The results for energies and errors are given in Table I. We see that for many cases the computed energy is not highly sensitive to the cancellation; the estimated error of around 1% is just what we would expect in the square (energy) of a quantity (amplitude) with an error of 0.5%. For some cases, however, especially those with higher  $\ell$ ,

there is a significant magnification of error. We emphasize that the error estimates given in Table I, are extremely conservative. In arriving at them we have used the maximum 0.5% error applied to all values of  $\omega$ , whereas this maximum error actually applies only to a small subset of the points. The smoothness of (most) waveforms reported in the next section, and the consistent variation of results with changing  $r_0$ , is evidence that the actual errors are rather smaller than those reported in Table I.

In addition to the infall from finite  $r_0$  we also have computed spectra and waveforms for infall from infinity. We characterize these cases with the same parameter  $\varepsilon_0$  we use for infall from  $r_0$ . Here it has the value of the Lorentz  $\gamma$ -factor

$$\varepsilon_0 \equiv 1/\sqrt{1-v_\infty^2} \quad (3.19)$$

for a particle with velocity  $v_\infty$  at infinity. For computation of infall from infinity the above computational scheme is modified only in the following ways: (i) The form of  $T(r)$  in (2.39) must be changed to

$$\begin{aligned} T(r) = & -\frac{\varepsilon_0}{\varepsilon_0^2-1} \left(\frac{r}{2M}\right) \sqrt{\varepsilon_0^2-1 + \frac{2M}{r}} \\ & - \frac{(2\varepsilon_0^2-3)\varepsilon_0}{(\varepsilon_0^2-1)^{3/2}} \ln \left[ \sqrt{(\varepsilon_0^2-1) \left(\frac{r}{2M}\right)} + \sqrt{1 + (\varepsilon_0^2-1) \left(\frac{r}{2M}\right)} \right] \\ & + \ln \left[ \frac{(2\varepsilon_0^2-1)(r/2M) + 1 + 2\varepsilon_0(r/2M) \sqrt{\varepsilon_0^2-1 + 2M/r}}{(r/2M) - 1} \right]. \end{aligned} \quad (3.20)$$

(ii) The initial value contributions in (3.18) must be omitted. (iii) The limit of integration in (3.12) must be changed from  $r_0^*$  to  $\infty$ . The computed energy for these  $\varepsilon_0 \geq 1$  cases are given in Table II. Since there is only a particle contribution in these cases, there is no issue of cancellation affecting the errors. The errors in the energy are, in fact, primarily due to the cutoff in the solution at a finite radius (with an analytic addition to represent the source contribution to infinity). Error estimates were made by varying the cutoff radius, and were found to be around 1% for all  $\varepsilon_0 \geq 1$  cases.

#### IV. WAVEFORMS AND SPECTRA

Results for quadrupole waveforms and spectra naturally divide themselves into three ranges, small  $r_0/2M$  (less than  $\sim 2$ ), moderate  $r_0/2M$  (from  $\sim 2$  to  $\sim 5$ ) and large  $r_0/2M$ . Waveforms are given as functions of retarded time  $u \equiv t - r^*$ . For small  $r_0$ , as shown in Fig. 1a, the shape of the waveform is that of simple quasinormal ringing. This shape is the same for all  $r_0$  and the single example shown suffices for all small  $r_0$ . Since the waveforms have the same shape, the energy spectra, shown in Fig. 1b,c, also have the same shape, changing only in magnitude as  $r_0$  increases.

As  $r_0$  increases further, the early negative excursion of the waveform begins to broaden, and the spectrum shifts slightly. Fig. 2 shows the  $r_0/2M = 2$  spectrum along with the spectra for the two limiting cases, the DRPP infall from rest at  $r_0 \rightarrow \infty$ , and the close-limit spectrum  $r_0 \rightarrow 0$ . (The latter is normalized to have the same energy as the  $r_0 = 2$  spectrum.) The  $r_0/2M = 2$  spectrum has an appearance that interpolates between the two limits, as might be expected. As  $r_0$  increases further, however, changes in the spectrum develop that might not be expected. As shown in Fig. 3, the simple spectrum for small  $r_0$  develops a secondary peak and the secondary peak grows with  $r_0$ . As  $r_0$  continues to increase, the initial shape of the waveform becomes a very broad depression extending from the moment infall begins to the beginning of quasinormal ringing. This is illustrated in the waveform in Fig. 4a, for  $r_0/2M = 10$ . The start of infall, at  $t = 0$ ,  $r_0/2M = 10$  corresponds to  $u/2M = -12.2$ , and it is at this value of  $u$  that the waveform begins to take on nonzero values. The initial part of the waveform, then, represents the gravitational bremsstrahlung from the early nonrelativistic part of the particle motion. The small wiggles around  $u/2M \approx -12$  are a numerical artifact due to imperfect cancellation of contributions from the initial value and particle parts of the source. (To verify this we changed the initial value contribution by  $\pm 10\%$  and found the change in the initial wiggles to be much greater than in other features of the waveform). For comparison, a DRPP waveform, for infall from infinity, is also shown in Fig. 4. (For infall from infinity, of course, the zero of time cannot be set to the beginning of infall. The time was arbitrarily shifted for the DRPP curve.) This waveform has a similar ringing pattern as the infall from finite radius, but lacks the initial waveform depression.

The end of the initial waveform depression is, roughly, the beginning of of quasinormal ringing, as can be seen in Fig. 4a. The generation of quasinormal ringing [18] is associated with the peak of the potential in (2.9). The time  $t/2M \approx 54$  at which the particle reaches the peak, at around  $r/2M \approx 1.5$  is at retarded time  $u/2M \approx 53$ . This is consistent with Fig. 4a, which shows ringing beginning somewhere around this value of  $u$ .

It is interesting to compare the waveforms for a particle falling from rest, to the waveform of a particle on a time-symmetric geodesic trajectory, a particle that long in the past was moving radially outward just outside a hole, that reaches a certain maximum radius  $r_0$  at time  $t = 0$ , and that subsequently falls into the hole. The analysis of this case requires only a simple modification of (3.13); the initial value terms are omitted and (due to time symmetry of the source) the complex conjugate of  $\mathcal{I}_1 + \mathcal{I}_2$  is added to  $\mathcal{I}_1 + \mathcal{I}_2$ . The resulting waveform is shown in Fig. 5a, and has also been given in Ref. [12]. That waveform shows two periods of quasinormal ringing, an early one excited when the particle goes outward through the region around the potential peak, and a later one due to motion inward through the peak. This later period of ringing, and in fact all features of the waveform generated after  $u/2M \approx -10$  agree very closely with the waveform for the particle falling from rest. Because the earlier ringing has a higher amplitude, the energy spectrum for the symmetric trajectory, shown in Fig. 5b, is dominated by this early ringing, and has very large amplitude. In the figure it is seen to be much larger than the DRPP spectrum, which (see Fig. 4) approximates the spectrum for infall from  $r_0/2M = 7.5$ .

Since the spectra for infall from both small  $r_0$  and from  $\infty$  have a single peak (see, e.g., Fig. 2) it is interesting that for intermediate values of  $r_0$  the spectra are characterized by a row of more-or-less evenly spaced bumps. As  $r_0$  grows, the number of bumps increases, and the bumps decrease in spacing and in height. The origin of these modulations can be understood by considering a simple example: Suppose a waveform consists of nothing but a single period of quasinormal ringing with the transform  $A(\omega)$ . The transform of the same waveform shifted later in time by  $T_{\text{shift}}$  would be  $A(\omega)e^{i\omega T_{\text{shift}}}$ . A wave consisting of *two* periods of ringing, the original and the later one, would then have a transform  $A(\omega)(1 + e^{i\omega T_{\text{shift}}})$ , and hence an energy spectrum

$$\omega^2 |A(\omega)|^2 4 \cos^2\left(\frac{1}{2}\omega T_{\text{shift}}\right) . \quad (4.1)$$

The combined spectrum would have the shape of the single waveform spectrum modulated on a frequency scale  $\delta\omega = 2\pi/T_{\text{shift}}$ . If the two waveforms were not identical, we would expect modulation of the spectrum, but less than 100% modulation.

This explanation can be tested on time-symmetric motion, where there are two well separated periods of ringing in in Fig. 5a. The amplitudes of the ringing are different, of course, so we shouldn't expect 100% modulation of the spectrum and, indeed, the modulations in Fig. 5b, are not 100%. The time shift between the first and second ringing periods is on the order of  $75(2M)$  (roughly the time it takes for the particle to rise up from  $r_0/2M = 1.5$  to  $r_0/2M = 7.5$  and fall back to  $r_0/2M = 1.5$ ). This suggests that the spacing of the spectral bumps should be  $\delta\omega = 2\pi/[75(2M)] = 0.84/2M$ , which is in good agreement with what is seen in Fig. 5b. The application to a nonsymmetric waveform, like that in Fig. 4a, is less obvious. The spacing of bumps  $\delta\omega \approx 0.11/2M$  in Fig. 4c suggests that the time shift is on the order of  $57(2M)$ . This, presumably, represents the time between the descent of the waveform at  $u/2M \approx 0$  and the start of ringing at  $u/2M \approx 50$ .

The interpretation works as well as a predictor of the bump spacing for other values of  $r_0$ , and seems clearly to be qualitatively correct, and to explain the progression of the spectra. As  $r_0$  approaches the horizon, the time between the initial moment and the onset of ringing goes to zero, so the spacing of bumps is infinite and there are no modulations of the spectrum. We get the single-humped close-limit spectrum. As  $r_0$  grows, the time between the initial motion and the start of ringing increases, so the spacing of the bumps gets smaller, and hence more bumps appear. As  $r_0$  is becoming larger, however, the early waveform is becoming less dramatic (the initial depression is decreasing in amplitude) so in interacting with the later ringing it is producing smaller modulation; the height of the bumps is decreasing. Finally, as  $r_0 \rightarrow \infty$ , we can think of the spectrum approaching one that has an infinite number of infinitesimally spaced zero-height bumps, bumps that are invisible in the DRPP spectrum.

Results for higher  $\ell$ -poles are shown in Figs. 6. The waveforms for  $\ell > 2$  show a more complicated structure of the pre-ringing radiation, resulting in more complex spectra. The total energy radiated in different  $\ell$ -poles is shown in Fig. 7. Results are given for several different values of  $r_0$ , and for particles falling in from infinity, both with no initial velocity (the DRPP case) and with  $\varepsilon_0 > 1$ . The distribution of energy among the multipoles is dominated by the quadrupole for small  $r_0$ . As  $r_0/2M$  increases to around 1.5, the higher multipoles become more important, but with further increase of  $r_0/2M$  to  $\sim 2$  the trend is reversed, and the ratio of multipole energies take on values that remain constant for further increases in  $r_0$ . For infall from infinity, the ultrarelativistic cases, with high  $\varepsilon_0$ , radiate more heavily in higher multipoles, as would be expected. To find the total energy, given in Fig. 8, we computed energy radiated in  $\ell = 2, 3, 4$  modes and assumed that the energies from each  $\ell$  decreased as a geometric series. This allowed us to add an estimate of the contributions from  $\ell > 4$ . The addition was typically around 2% of the energy. The energy is plotted as a function of proper distance  $L = \int_{2M}^{r_0} dr/\sqrt{1 - 2M/r}$ , rather than  $r_0$ , to show more clearly the details for small separation.

Aspects of infall from infinity are given in Fig. 9, which shows waveforms and spectra. The waveforms are characterized by a large early amplitude that is an increasing function of  $\varepsilon_0$ , and the spectra show strong low frequency radiation, extending to  $\omega = 0$ , due to this early phase of the radiation. The total energy radiated in the lowest three

multipoles is also shown. (Since the relative importance of higher multipoles increases with  $\varepsilon_0$ , extrapolation to total radiated energy is not immediate.) The energy results are extended to include infall from finite radius where  $\varepsilon_0$  takes the value  $\sqrt{1 - 2M/r_0}$ .

## V. DISCUSSION

One of the interesting questions that can be clarified with the above results is the validity of the close approximation. This approximation, for two holes, assumes that the holes are initially close enough so that the structure of the initial data at small radius is inside an initial all-encompassing horizon. Only the large  $r$  features of the initial data therefore are relevant to the production of outgoing radiation. We can immediately apply this method to the particle problem by comparing our initial geometry, in (2.23) and (2.21), with the initial geometry in equation (4.25) of Ref. [12]. We see that the results of that reference can be applied to the particle problem by the replacement

$$8M\kappa_\ell(\mu_0) \rightarrow m_2(z_2/M)^\ell. \quad (5.1)$$

With (2.25) and (2.27) this can be rewritten as

$$\kappa_\ell(\mu_0) \rightarrow \frac{1}{2^{\ell+2}} \left(\frac{m_0}{2M}\right) \left(\frac{r_0}{2M}\right)^\ell \left(1 + \sqrt{1 - 2M/r_0}\right)^{2\ell+1}. \quad (5.2)$$

By the methods of Refs. [12,14],  $E_\ell/2M$ , the radiated energy in units of  $2M$ , for each multipole, is shown to be  $1.26 \times 10^{-2}\kappa_2^2$ ,  $3.10 \times 10^{-3}\kappa_3^2$ ,  $8.33 \times 10^{-4}\kappa_4^2, \dots$ , respectively for  $\ell = 2, 3, 4 \dots$ . If we replace  $\kappa_\ell$  with (5.2) we find the close limit predictions for energy. In Refs. [12,14] the outgoing radiation is computed from an evolution of  $\psi_\ell$ , using a finite difference representation of (2.8) (with no source term). Here we have also computed waveforms and energies in the close limit directly by the transform methods of Secs. II and III, with only the following changes: The integrals  $\mathcal{I}_1 + \mathcal{I}_2$  are omitted from (3.13), and only the  $\bar{r} > z_2$  form of  $\mathcal{F}_\ell(\bar{r})$  is used in (2.21). The results of the two methods are energy values that agree to better than 1% and waveforms that are almost indistinguishable. (The numerically evolved waveforms are rather smoother than the waveforms from the transform method. They lack the small amplitude wiggles that can be seen, e.g., in the waveform in Fig. 1a at early times.)

In Fig. 10, we plot the  $\ell = 2$  close-limit energy prediction and compare it to the full computation for the particle infall. It is clear that the close limit method is acceptable out to  $r_0 \approx 2.2M - 2.3M$ , and fails by a large factor at  $r_0 = 3M$ . This is in accord with the general picture that the close limit should be a reasonably good approximation when the particle starts inside the peak, around  $r \approx 3M$ , of the potential (2.9). The waveforms in the close limit all have precisely the same shape; only the amplitudes differ. The computed waveforms are in excellent agreement with the small  $r_0$  waveforms (see, e.g., the waveforms for  $r_0/2M = 1.5$  in Fig. 1a). The close-limit predictions of waveform shape are even better than the energy predictions. Only for  $r_0/2M$  larger than around 1.5 does the waveform start to change from the close-limit shape.

The dependence of radiated energy on  $r_0$ , shown in Fig. 8, is perhaps the most interesting result of our computations. One has an intuitive instinct that the radiated energy should decrease with decreasing  $r_0$ . At the crudest level this intuition is based on the idea that infall from a larger radius results in a particle which “strikes” the black hole harder and excites more quasinormal ringing. Since a decrease of energy with smaller  $r_0$  is expected, a natural first guess for approximating the decrease is to multiply the DRPP energy by a reduction factor  $(1 - k2M/r_0)$ , where  $k$  is some fitting parameter of order unity. This approximation, with  $k = 1.5$  is shown in Fig. 11 and is compared with the computed results, and with the DRPP limit. The choice  $k = 1.5$  was made to give good agreement at  $r_0/2M = 15$ , and presumably at larger values of  $r_0$ . (It is difficult to compute energies at much larger values of  $r_0$ , due to the rapid modulation of the spectrum.)

A more physical justification for decrease of radiation with decreasing  $r_0$  can be constructed starting with the quadrupole formula. A faster moving particle from a larger  $r_0$  implies a larger value of the time derivatives of the quadrupole moment. This argument has been used [19] as the basis of a simple quantitative model for the effect of varying  $r_0$ . The energy for infall from infinity, in that model, is reduced by a reduction factor  $F_{r_0}$  based on the quadrupole formula. [See eq. (23) of Ref. [19].] (For large  $r_0$  that reduction factor reduces to  $F_{r_0} = 1 - (60/27)(2M/r_0) + \mathcal{O}(2M/r_0)^2$ .) In Fig. 11, we show the result of that simple model. It is clear that the  $F_{r_0}$  factor captures the correct qualitative feature of a decrease of radiation with decrease of  $r_0$  but implies too dramatic a decrease.

As  $r_0$  continues to decrease, a rather unexpected effect appears. Below  $r_0 \approx 7M$  the energy begins to increase with decreasing separation. At yet smaller radii ( $r_0$  less than around  $4.5M$ ) the energy again decreases with decreasing  $r_0$ , as the close limit dictates it must. Thus the relationship of radiated energy and  $r_0$  has the expected nature in

the two regimes where simple arguments apply: large separations and small separations. The anomalous behavior in the range  $4.5M-7M$  underscores the fact that the generation of outgoing radiation is tied closely to the nature of the potential (2.9), which peaks around  $r_0 = 3M$ , and cannot be understood in terms of close or far approximations. This anomaly, it should be noted, appears to have no equivalent feature in the case of the head-on collision of two equal mass holes [12]. Presumably this is because the replacement of the particle by a hole means that the infalling hole is not localized at a particular value of the potential of the other hole. As the mass ratio of the infalling holes becomes smaller and smaller there must come a point at which an anomalous bump develops in the dependence of radiation on initial separation.

We have seen that the particle limit provides a relatively easy tool for understanding some aspects of the generation of radiation, and of the collisions of holes. We intend next to use this formalism to study what features on initial data are important to determining how much energy is radiated for particle infall, and presumably for black hole collisions.

### ACKNOWLEDGMENTS

This work has been partially supported by the National Science Foundation under grant PHY0507719. We thank Eric Poisson for useful discussions of computational aspects of the problem.

- 
- [1] M. Davis, R. Ruffini, W. H. Press, and R. H. Price, *Phys. Rev. Lett.* **27**, 1466, (1971) (“DRPP”).
  - [2] L. I. Petruch, S. L. Shapiro, and I. Wasserman, *Astrophys. J. Suppl. Ser.* **58**, 297, (1985).
  - [3] F. J. Zerilli, *Phys. Rev. Lett.* **24** 737 (1970).
  - [4] V. Moncrief, *Ann. Phys. (NY)* **88**, 323 (1974).
  - [5] R. Ruffini, *Phys. Rev.* **D7**, 972 (1973); V. Ferrari and R. Ruffini, *Physics Letters*, **98B**, 381 (1981).
  - [6] A. A. Abramovici *et al.*, *Science* **256**, 325 (1992); K. S. Thorne, submitted to *Proceedings of Snowmass 94 Summer Study on Particle and Nuclear Astrophysics and Cosmology*, eds. W. W. Kolb and R. Peccei (World Scientific, Singapore).
  - [7] Proceedings of the November 1994 meeting of the Grand Challenge Alliance to study black hole collisions may be obtained by contacting E. Seidel at NCSA (unpublished).
  - [8] P. Anninos, D. Hobill, E. Seidel, L. Smarr, W.-M. Suen, *Phys. Rev. Lett.* **71**, 2851 (1993).
  - [9] A. M. Abrahams, S. L. Shapiro, and S. A. Teukolsky, *Phys. Rev.* **D51**, 4295, (1995).
  - [10] T. Regge and J. A. Wheeler, *Phys. Rev.* **108**, 1063 (1957).
  - [11] C. W. Misner, K. S. Thorne and J. A. Wheeler, *Gravitation* (Freeman, San Francisco, 1973).
  - [12] P. Anninos, R. H. Price, J. Pullin, E. Seidel, and W.-M. Suen, *Phys. Rev.* **D52**, 4462 (1995).
  - [13] C. T. Cunningham, R. H. Price, and V. Moncrief, *Astrophys. J* **230**, 870 (1979).
  - [14] R. H. Price and J. Pullin, *Phys. Rev. Lett.* **72**, 3297 (1994).
  - [15] D. R. Brill and R. W. Lindquist, *Phys. Rev.* **131**, 471 (1963).
  - [16] A. Abrahams and R. H. Price, *Phys. Rev.* **D53**, 1972 (1996).
  - [17] F. J. Zerilli, *Phys. Rev.* **D2** 2141 (1970).
  - [18] C. T. Cunningham, R. H. Price, and V. Moncrief, *Astrophys. J* **224**, 643 (1978).
  - [19] P. Anninos, D. Hobill, E. Seidel, L. Smarr and W.-M. Suen, *Phys. Rev.* **D52**, 2044 (1995).

FIG. 1. The  $\ell = 2$  waveforms and spectra for small  $r_0$ . In (a) the waveform is shown as a function of retarded time  $u \equiv t - r^*$ , with  $t = 0$  corresponding to the moment at which the infall begins. Included for comparison is the predictions of the close-limit approximation. For the  $r_0/2M = 1.1$  case, shown in (b), the close-limit energy is larger than the computed energy by 11%. For the  $r_0/2M = 1.5$  case, in (c), the close-limit energy is 2.9 times the computed energy.

FIG. 2. The  $\ell = 2$  spectra for  $r_0/2M = 2$ , and for the two limiting cases: DRPP and close-limit. The close-limit case is normalized to have the same energy as the  $r_0/2M = 2$  spectrum. For the three spectra, close-limit,  $r_0/2M = 2$ , and DRPP, the maximum of the spectra occur respectively at  $\omega_{\max}(2M) = 0.765, 0.675$ , and  $0.625$ .

FIG. 3. Spectra of  $\ell = 2$  energy for  $r_0 = 3.5$  and  $4$ . For comparison, the DRPP spectrum for infall from infinity is also shown.

FIG. 4. The  $\ell = 2$  waveforms and spectra for large  $r_0$ . In (a) the waveform for  $r_0/2M = 10$  is shown as a function of retarded time  $u$ , and is contrasted with the DRPP waveform (for which the zero of retarded time has a different meaning). Energy spectra are shown in (b)–(d) for three large values of  $r_0$  and are contrasted with the  $r_0 \rightarrow \infty$  DRPP limit (dashed curves).

FIG. 5. The  $\ell = 2$  waveform and spectrum for a time-symmetric trajectory. In (a) the waveform (dotted curve) is given for a particle that moves outward and reaches a maximum at  $r_0/2M = 7.5$  before falling inward, and is compared with the waveform for infall from  $r_0/2M = 7.5$ . In (b) the spectrum of energy generated by the time-symmetric motion is compared with the DRPP spectrum for infall from infinity. The DRPP spectrum contains less than 5% as much energy as that for the time-symmetric motion.

FIG. 6. Results for higher multipole moments. For  $r_0/2M = 5$ , waveforms and spectra are shown for  $\ell = 2, 3, 4$ . Dashed curves are spectra for infall from infinity.

FIG. 7. Energy in different multipoles. Energy for  $\ell = 2, 3, 4$  is shown for several values of  $r_0$  in the case of infall from finite radius, and for several different values of  $\varepsilon_0$  in the case of infall from infinity. The energies for  $r_0/2M = 1.01$  are multiplied by 10 to improve the plot.

FIG. 8. Total energy radiated by a falling particle, as a function of the initial proper distance of the particle from the horizon. The points shown are at  $r_0/2M = 1.01, 1.1, 1.2, 1.3, 1.5, 1.8, 2, 2.25, 2.5, 2.75, 3, 3.5, 4, 5, 6, 7.5, 10, 15$ . The local maximum is at  $r_0/2M \approx 2.25$  and the minimum at  $r_0/2M \approx 3.5$ .

FIG. 9. Results for infall from infinity. Plots are given of waveforms (a) and spectra (b), (c), for a particle falling in from infinity with nonzero energy. The total radiation emitted in the first three multipoles is shown as a function of  $\varepsilon_0$ . This curve also extends to particles falling from finite radius, with  $\varepsilon_0 = (1 - 2M/r_0)^{1/2}$ . The local maximum of the spectrum occurs for  $\varepsilon_0 \approx 0.75$ , and the local minimum at about  $\varepsilon_0 \approx 0.84$ .

FIG. 10. Quadrupole energy for an infalling particle as a function of the particle's initial proper distance from the horizon. The computed energy is compared with the close-limit approximation.

FIG. 11. Total radiated energy as a function of  $r_0/2M$ . Computed results are compared with a simple model, and with the best  $1/r_0$  fit.

TABLE I. Radiated energy for infall from  $r_0$ 

$r_0/2M$	$\ell$	$(2M/m_0^2)E_\ell$	error
15	2	$1.64 \times 10^{-2}$	1%
	3	$1.98 \times 10^{-3}$	1%
	4	$2.88 \times 10^{-4}$	5%
5	2	$1.43 \times 10^{-2}$	1%
	3	$1.62 \times 10^{-3}$	2%
	4	$2.23 \times 10^{-4}$	6%
3	2	$1.40 \times 10^{-2}$	2%
	3	$1.65 \times 10^{-3}$	4%
	4	$2.61 \times 10^{-4}$	11%
2	2	$1.49 \times 10^{-2}$	3%
	3	$2.21 \times 10^{-3}$	5%
	4	$3.56 \times 10^{-4}$	11%
1.5	2	$8.11 \times 10^{-3}$	3%
	3	$2.10 \times 10^{-3}$	5%
	4	$5.66 \times 10^{-4}$	10%
1.1	2	$9.02 \times 10^{-4}$	< 1%
	3	$1.85 \times 10^{-4}$	1%
	4	$4.06 \times 10^{-5}$	4%

TABLE II. Radiated energy for infall from infinity

$\varepsilon_0$	$(2M/m_0^2)E_2$	$(2M/m_0^2)E_3$	$(2M/m_0^2)E_4$
1	$1.82 \times 10^{-2}$	$2.18 \times 10^{-3}$	$2.96 \times 10^{-4}$
1.1	$2.75 \times 10^{-2}$	$3.48 \times 10^{-3}$	$5.06 \times 10^{-4}$
1.3	$6.48 \times 10^{-2}$	$9.90 \times 10^{-3}$	$1.73 \times 10^{-3}$
1.5	$1.285 \times 10^{-1}$	$2.40 \times 10^{-2}$	$5.21 \times 10^{-3}$
1.8	$2.70 \times 10^{-1}$	$6.34 \times 10^{-2}$	$1.76 \times 10^{-2}$
3	1.285	$4.463 \times 10^{-1}$	$1.885 \times 10^{-1}$

Figure 1a

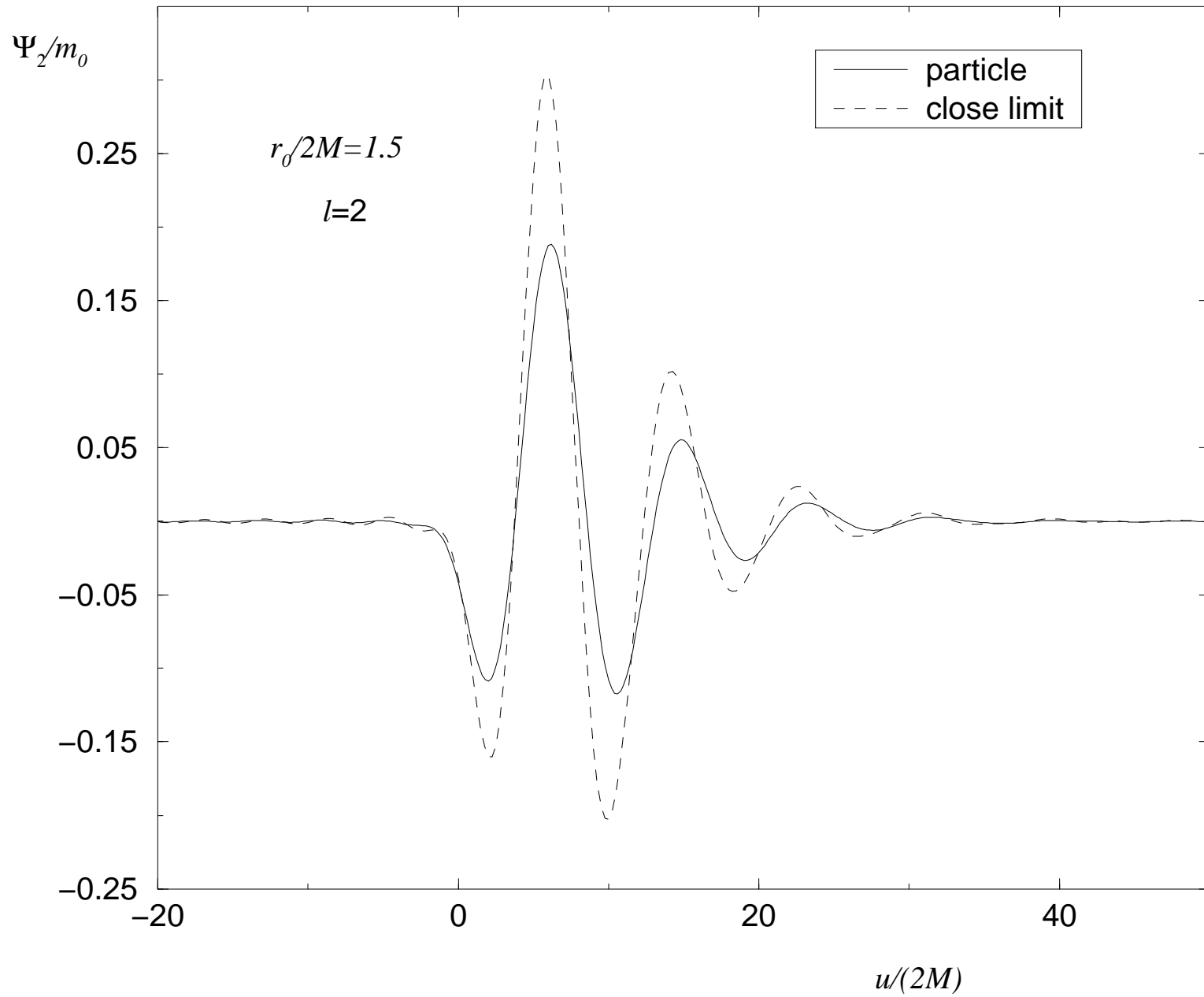


Figure 1b

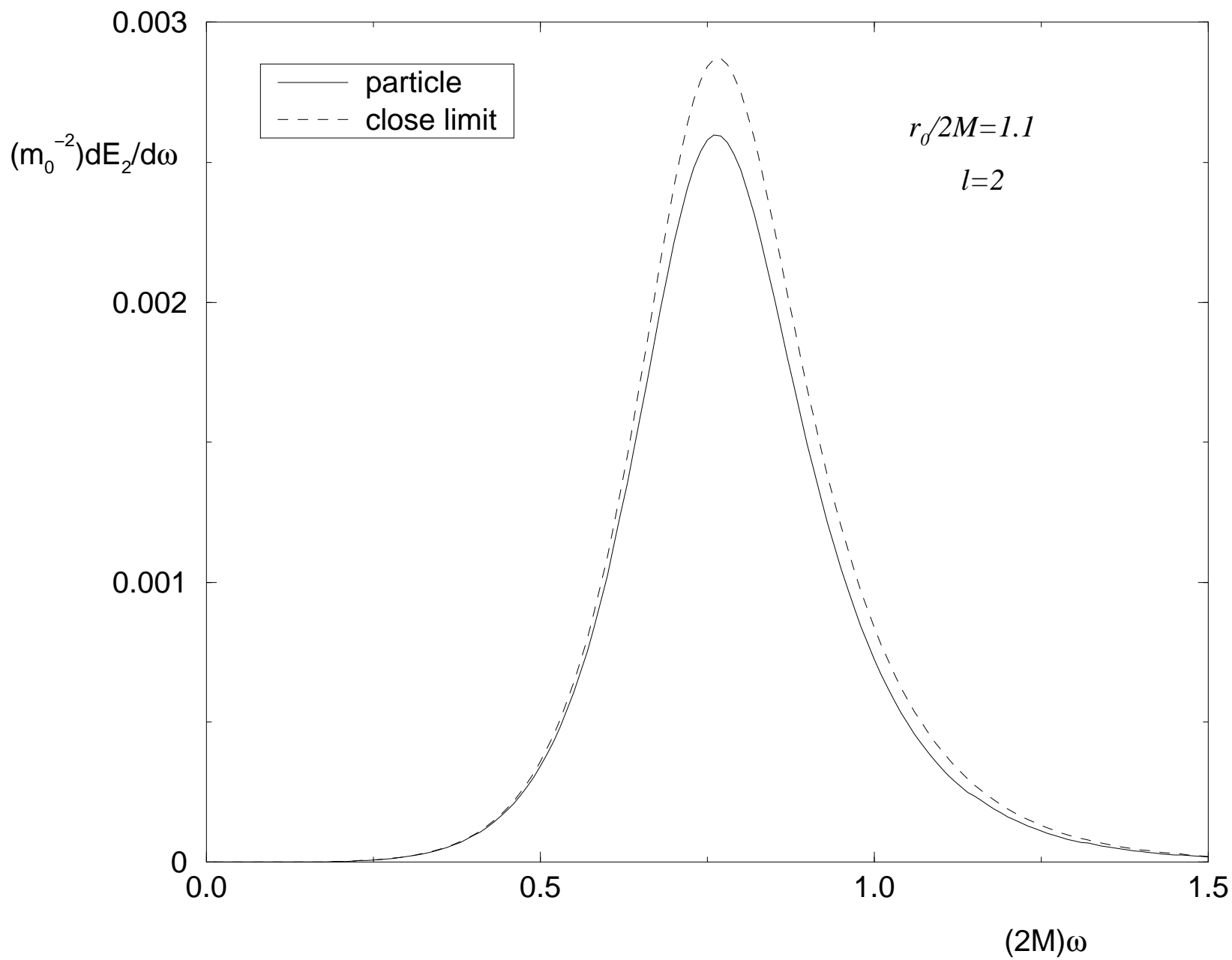


Figure 1c

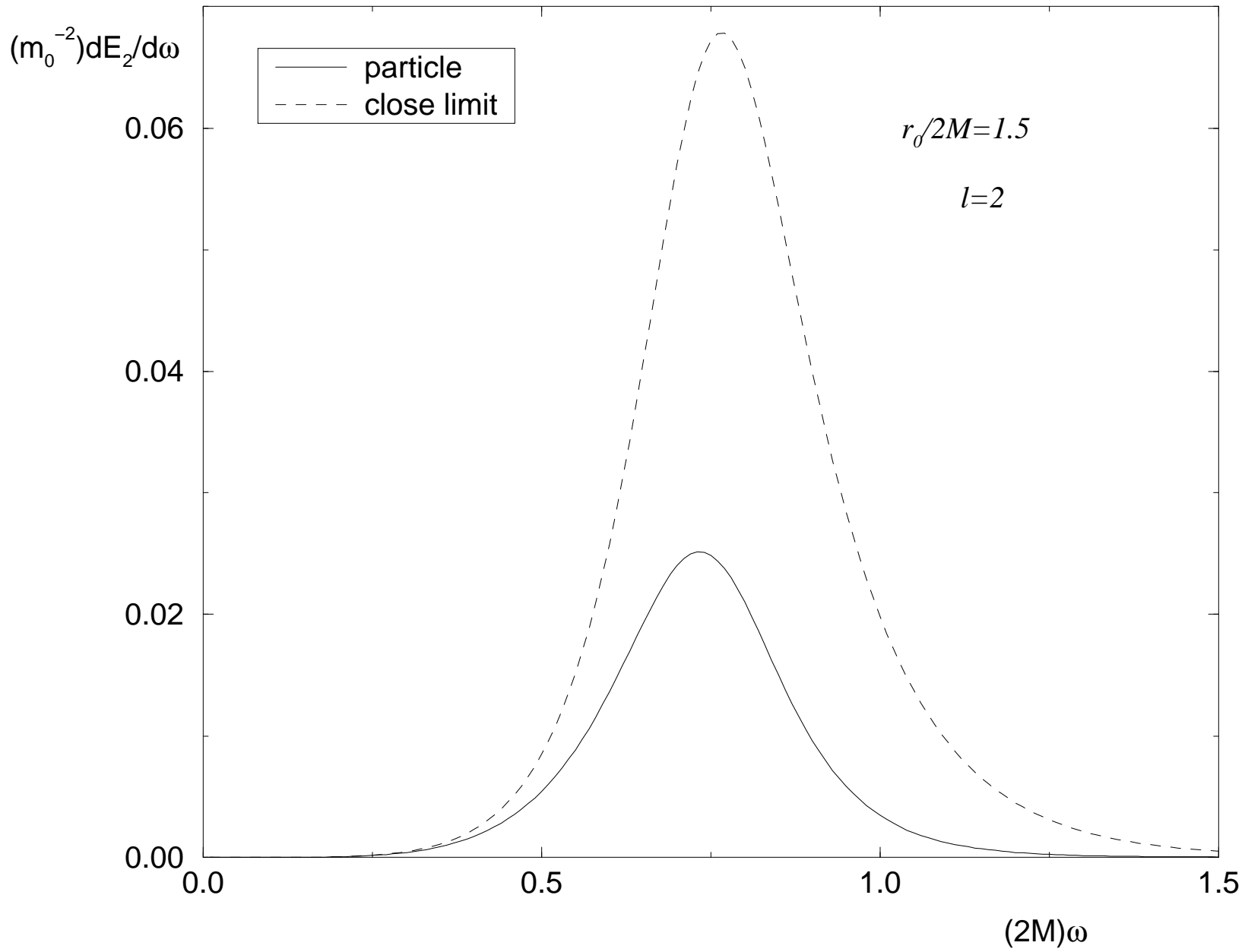


Figure 2

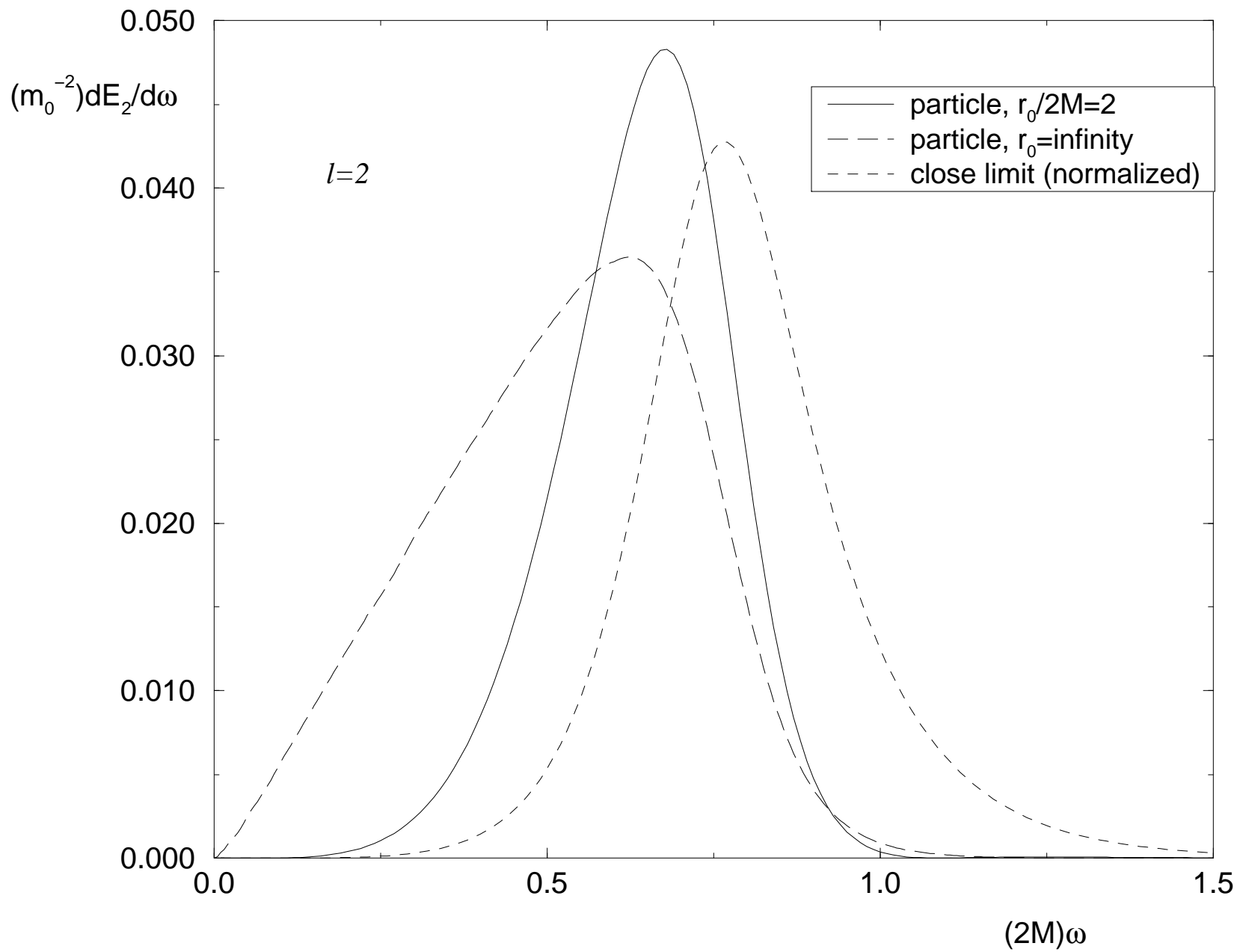


Figure 3

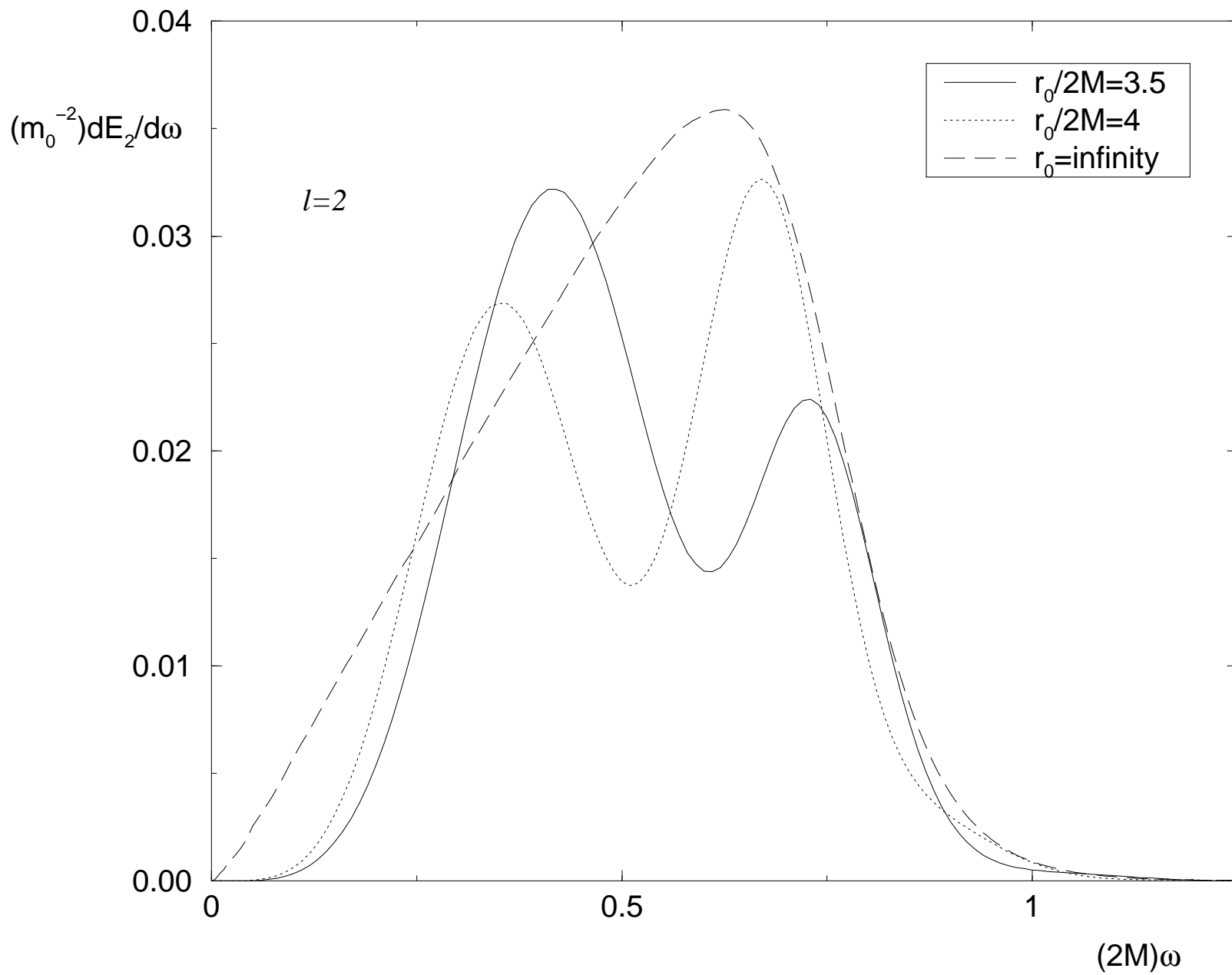


Figure 4a

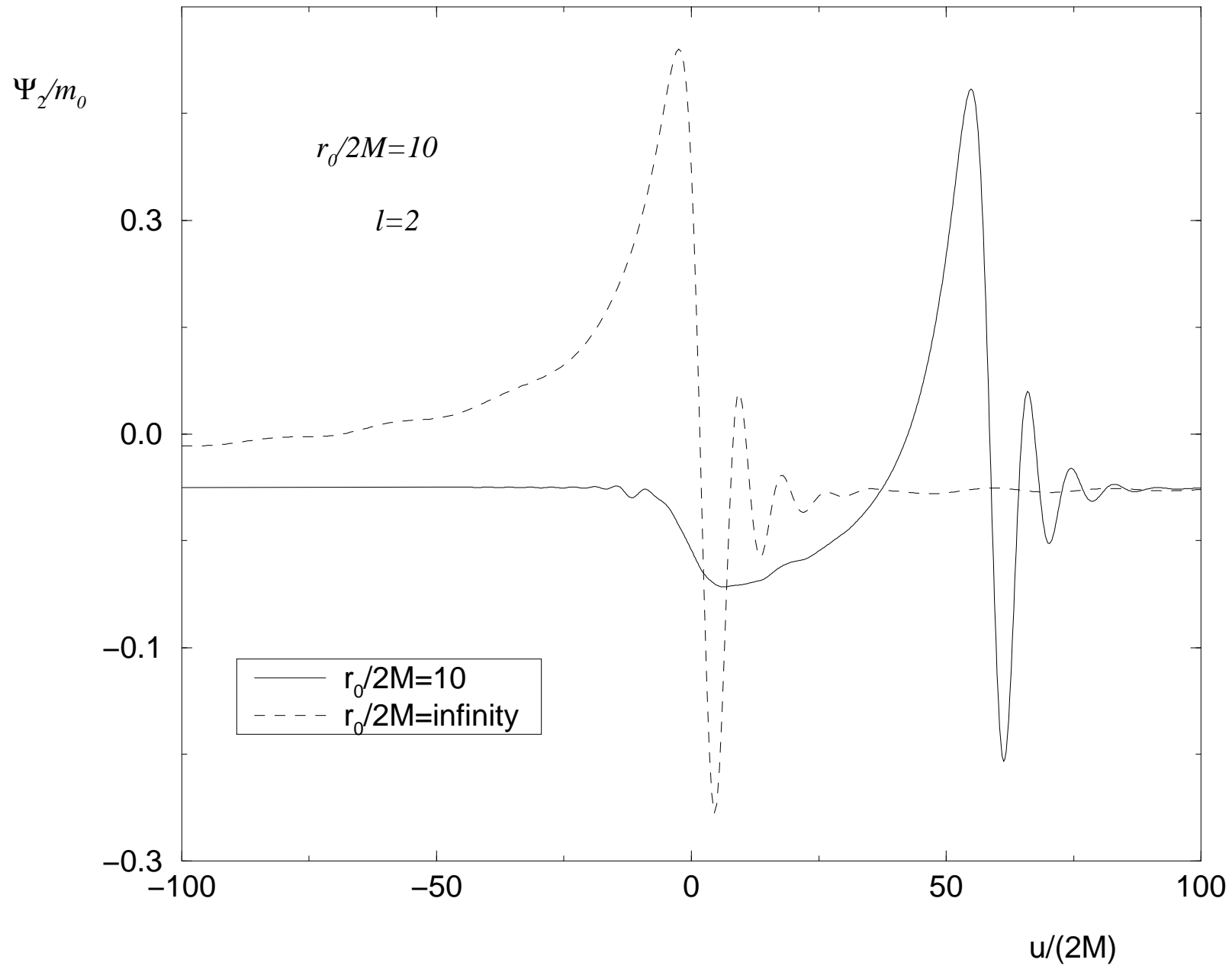


Figure 4b

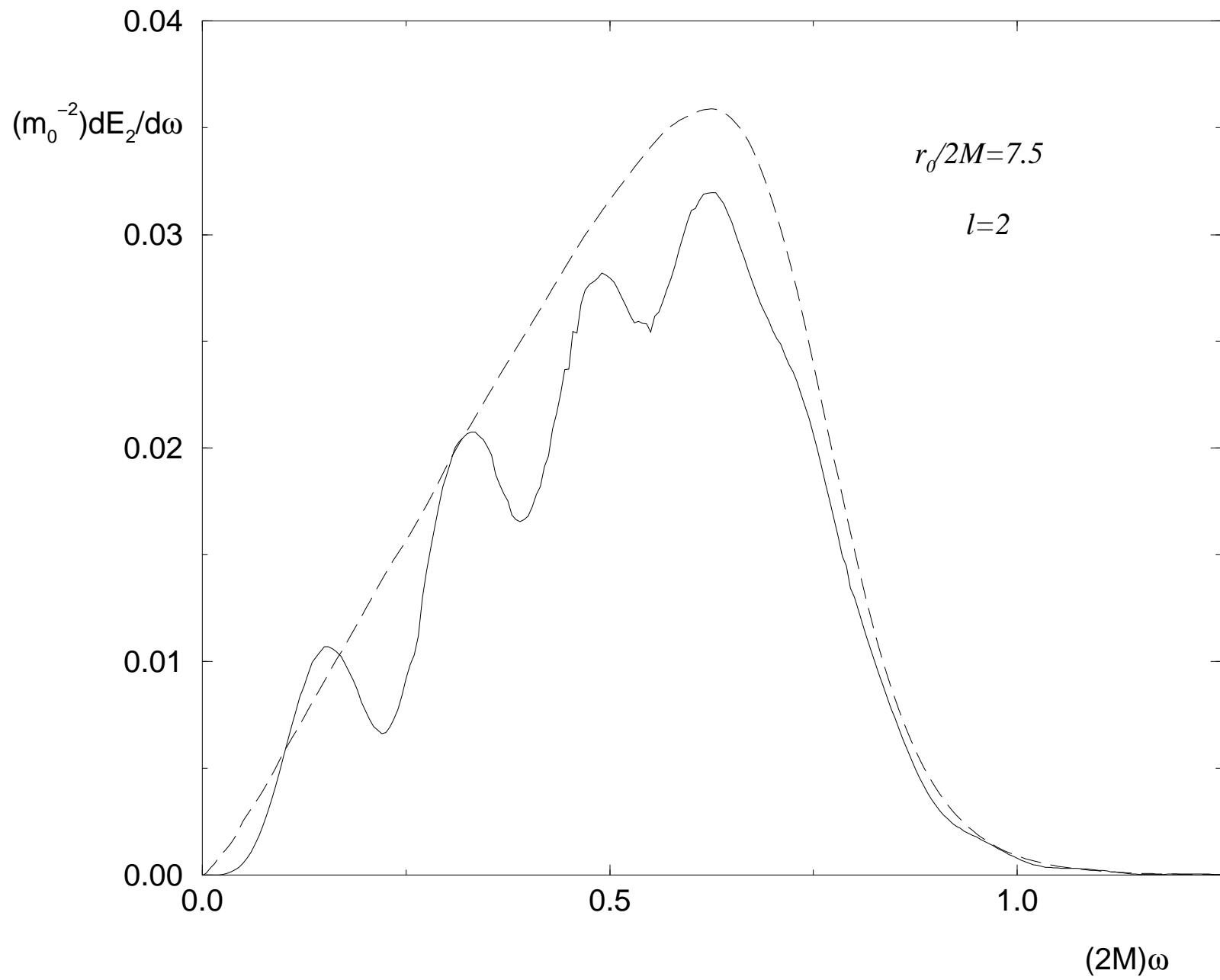


Figure 4c

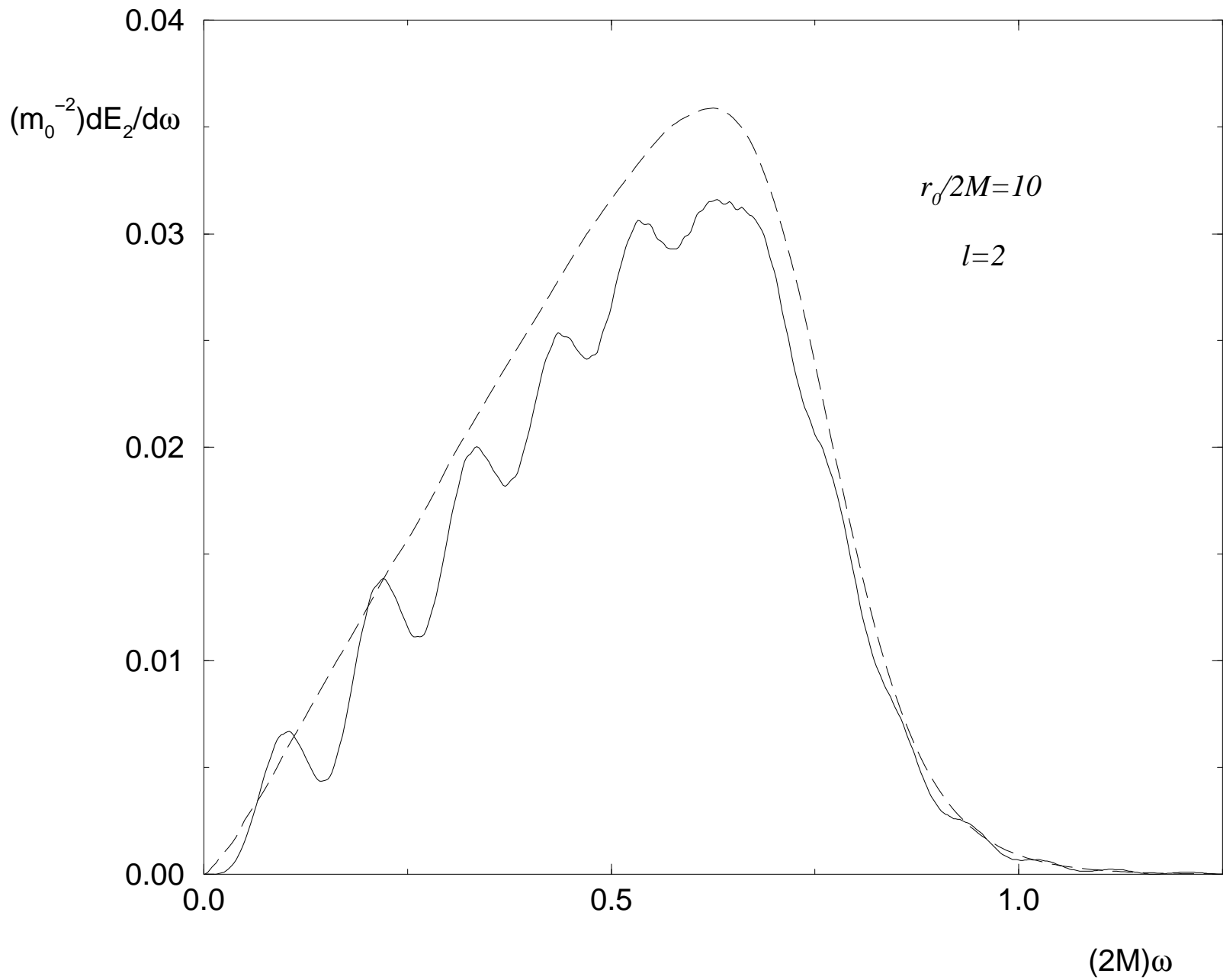


Figure 4d

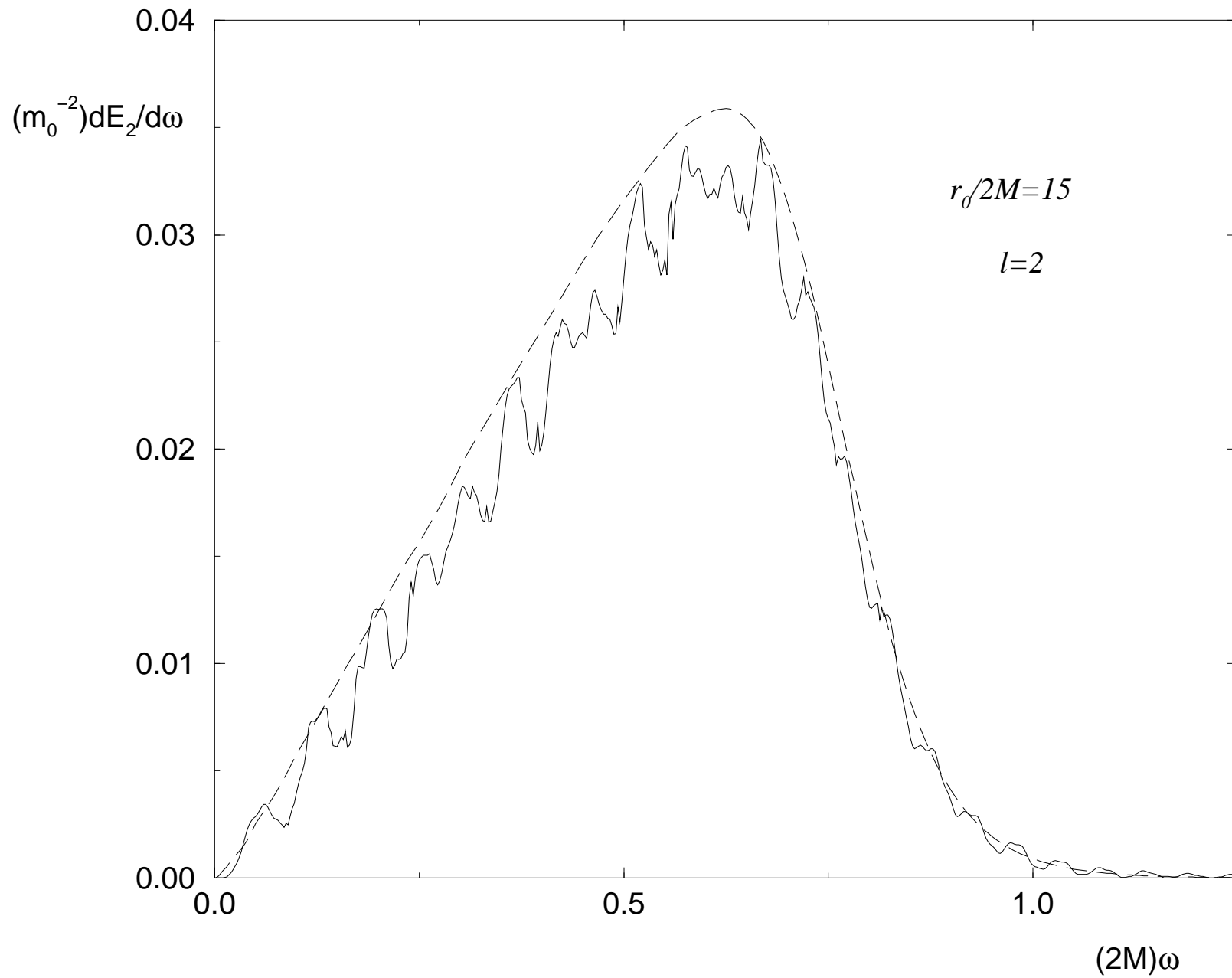


Figure 5a

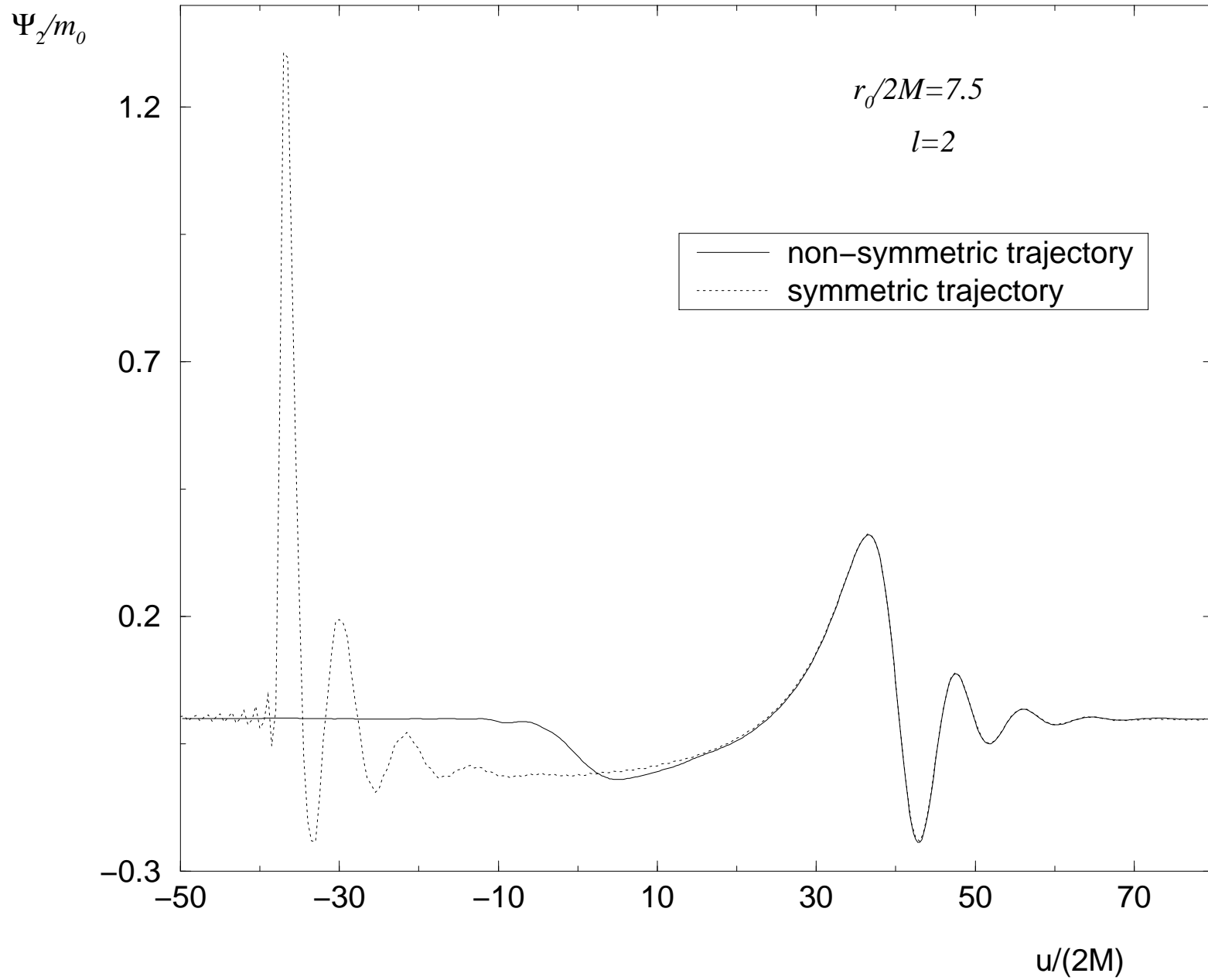


Figure 5b

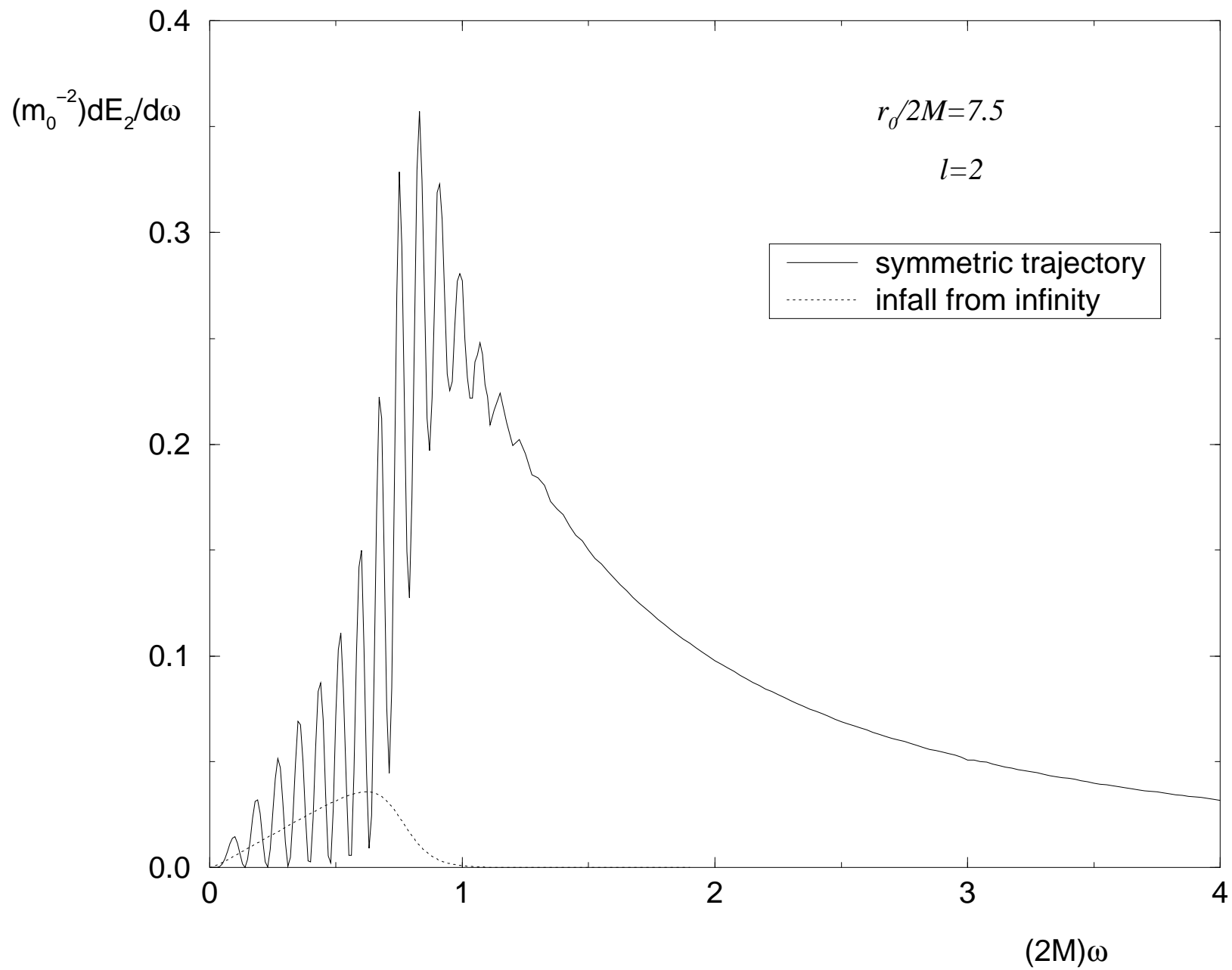


Figure 6a

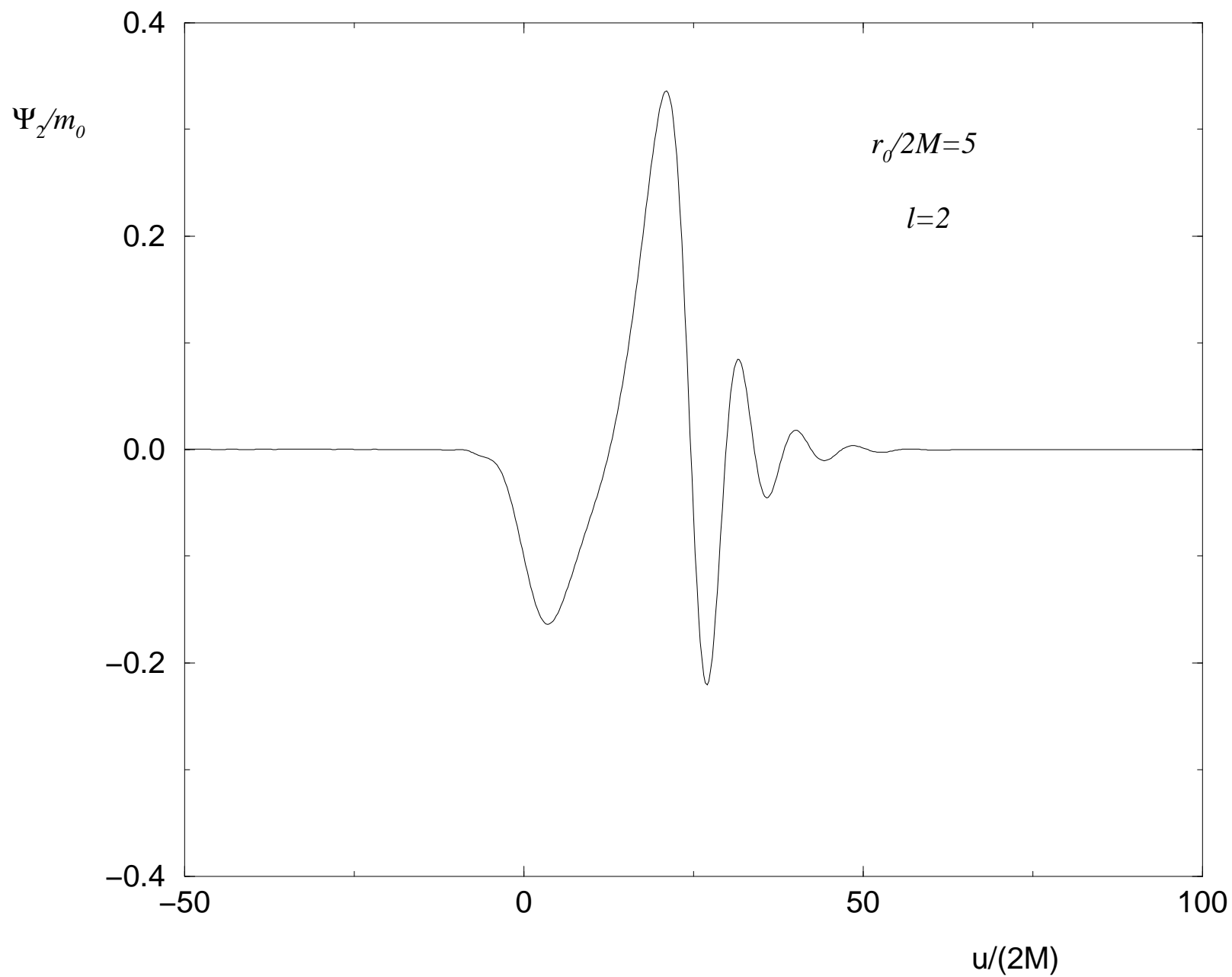


Figure 6b

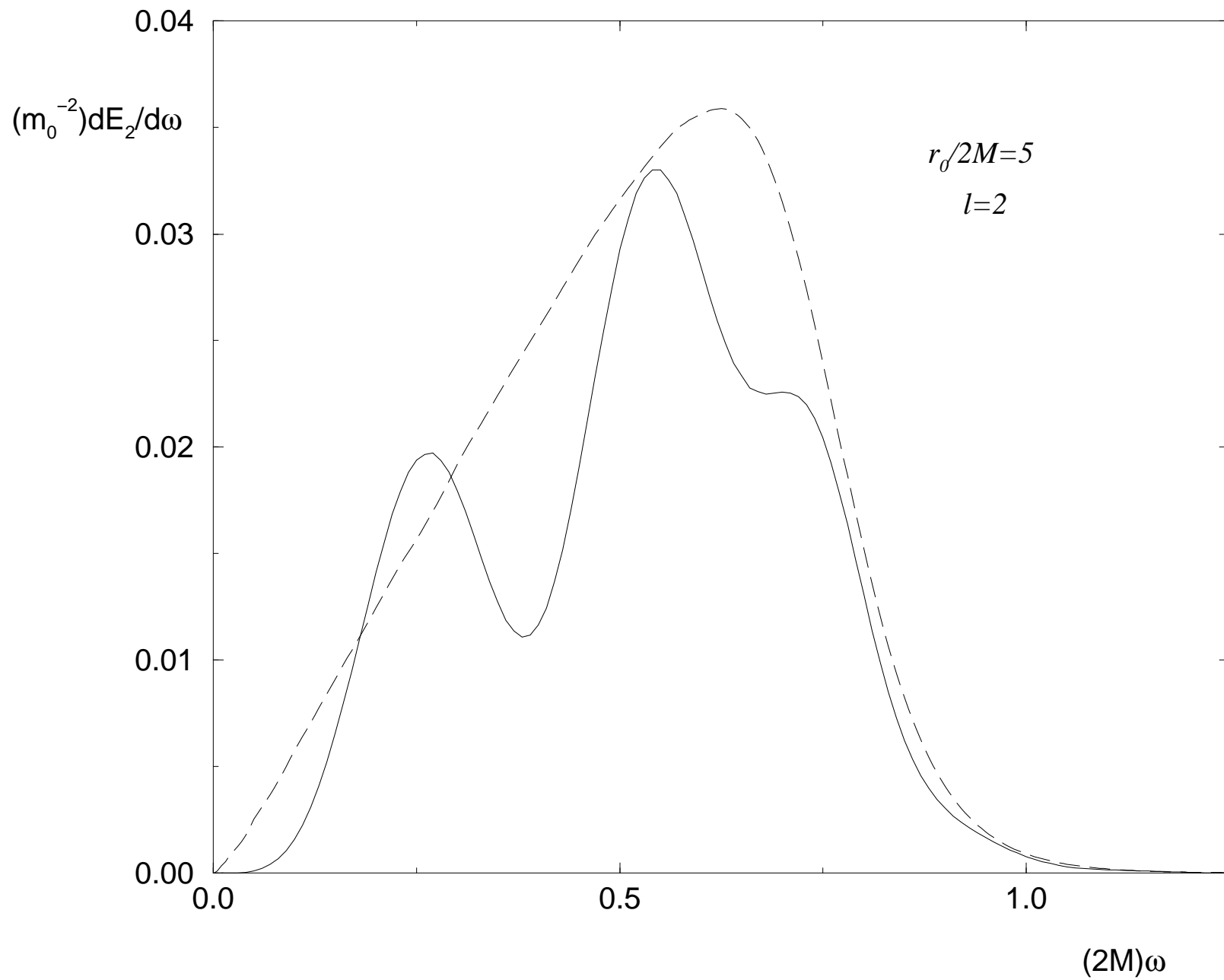


Figure 6c

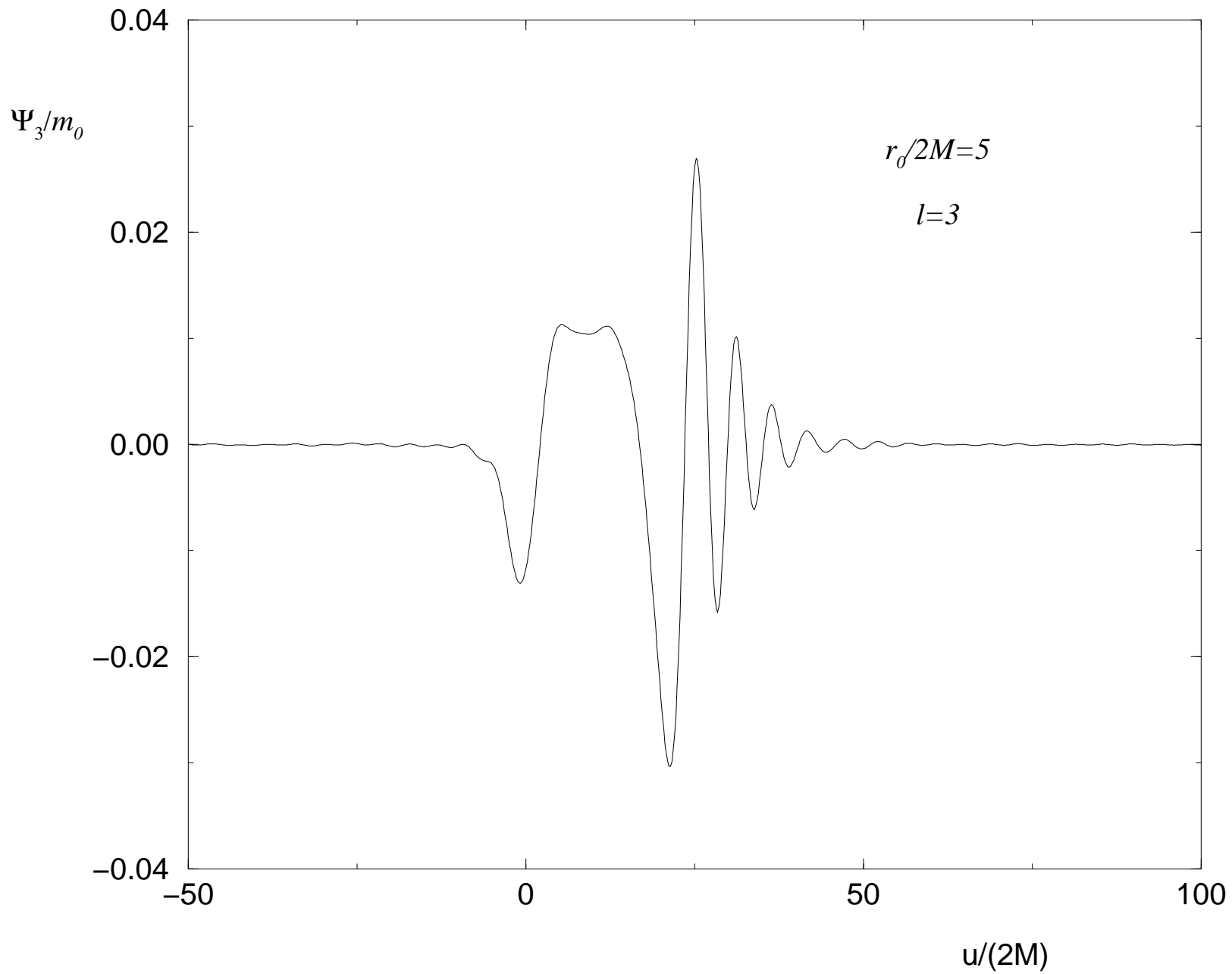


Figure 6d

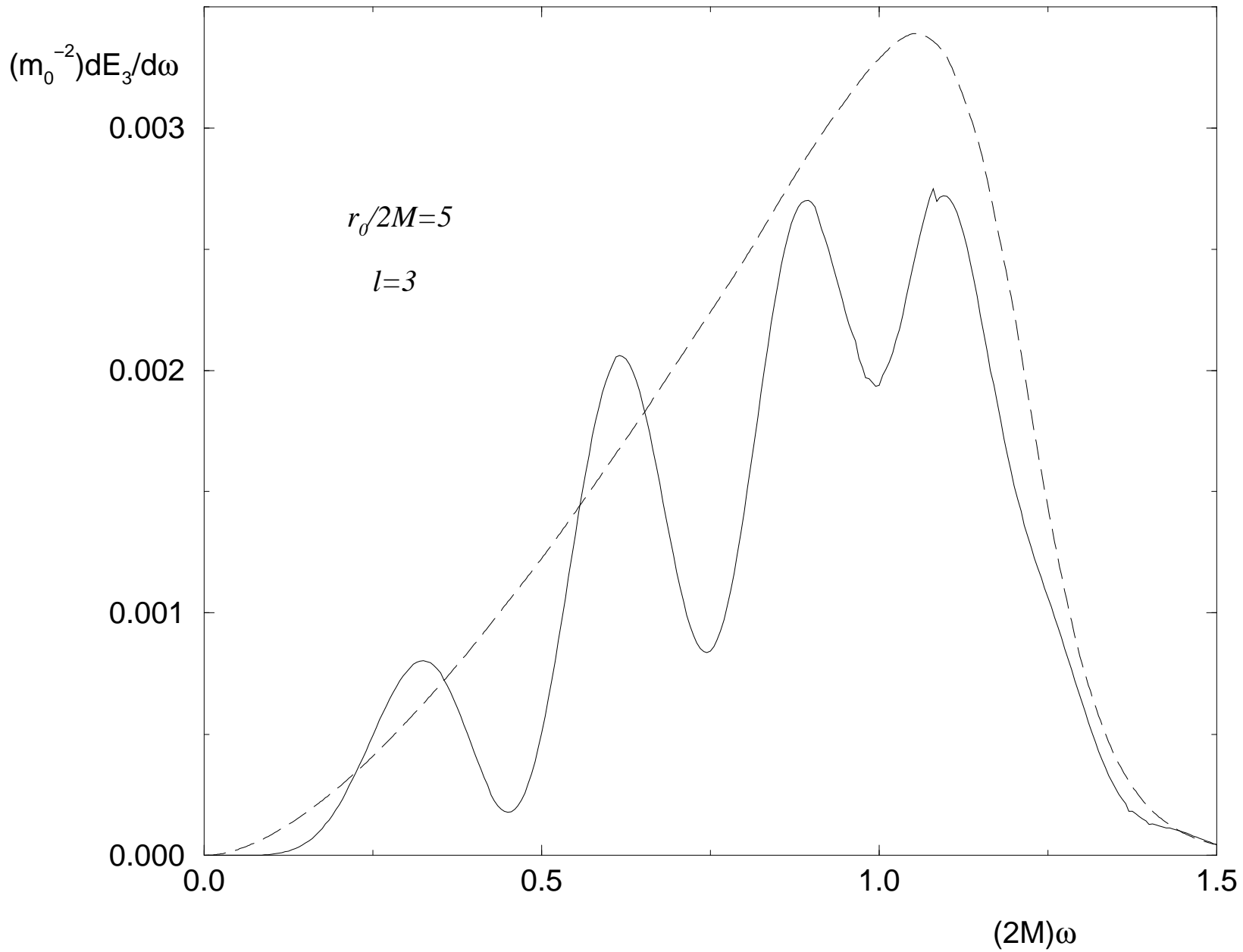


Figure 6e

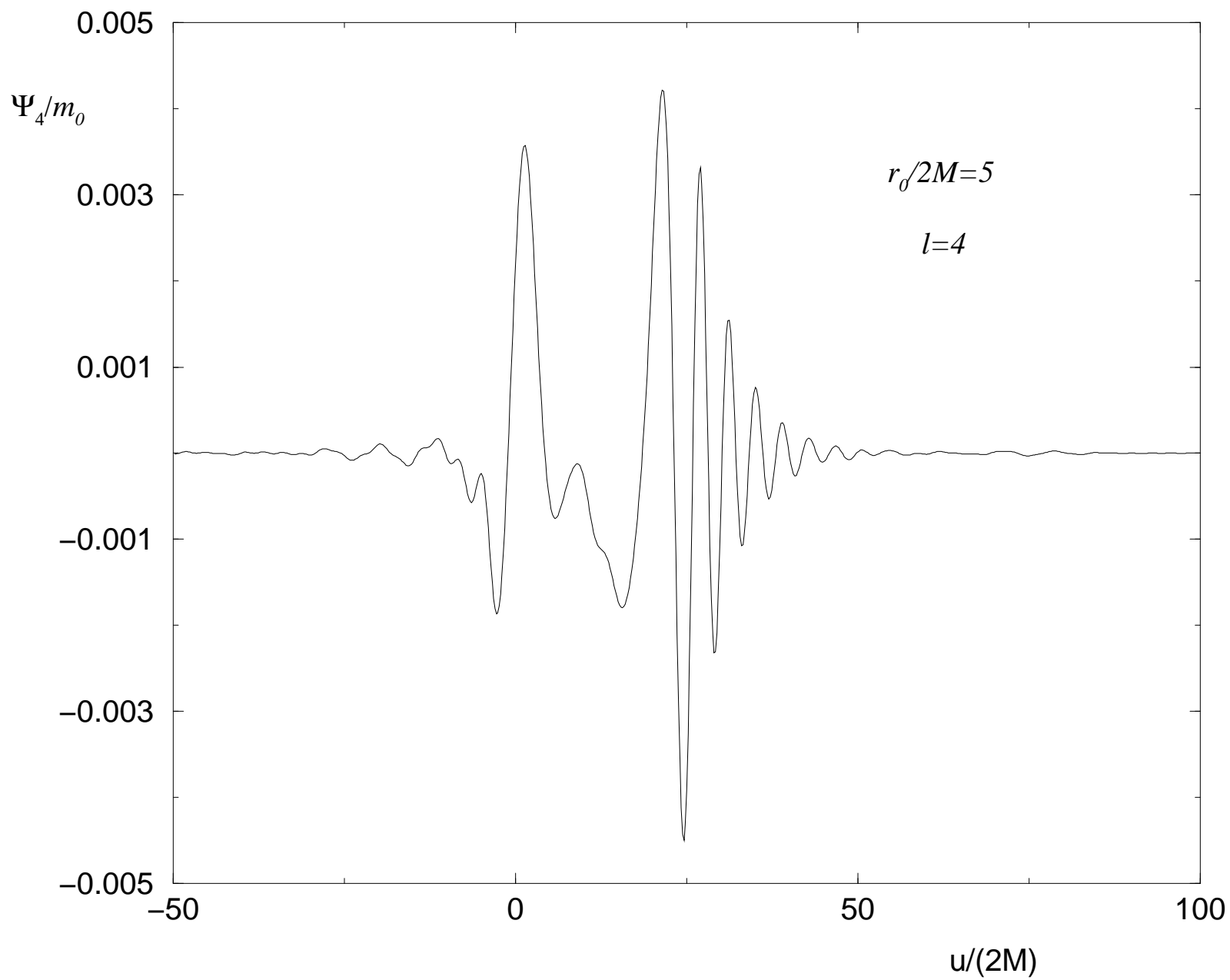


Figure 6f

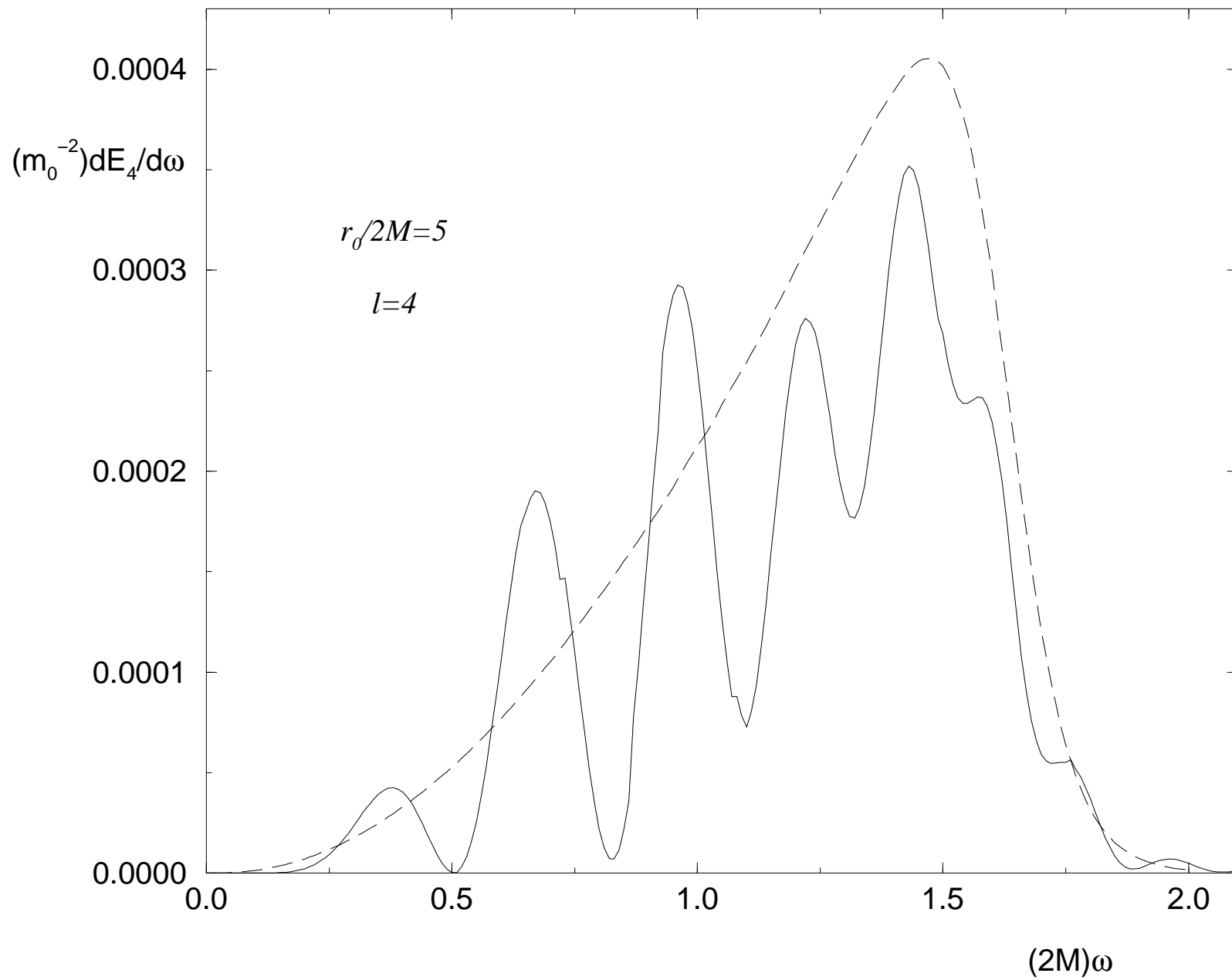


Figure 7

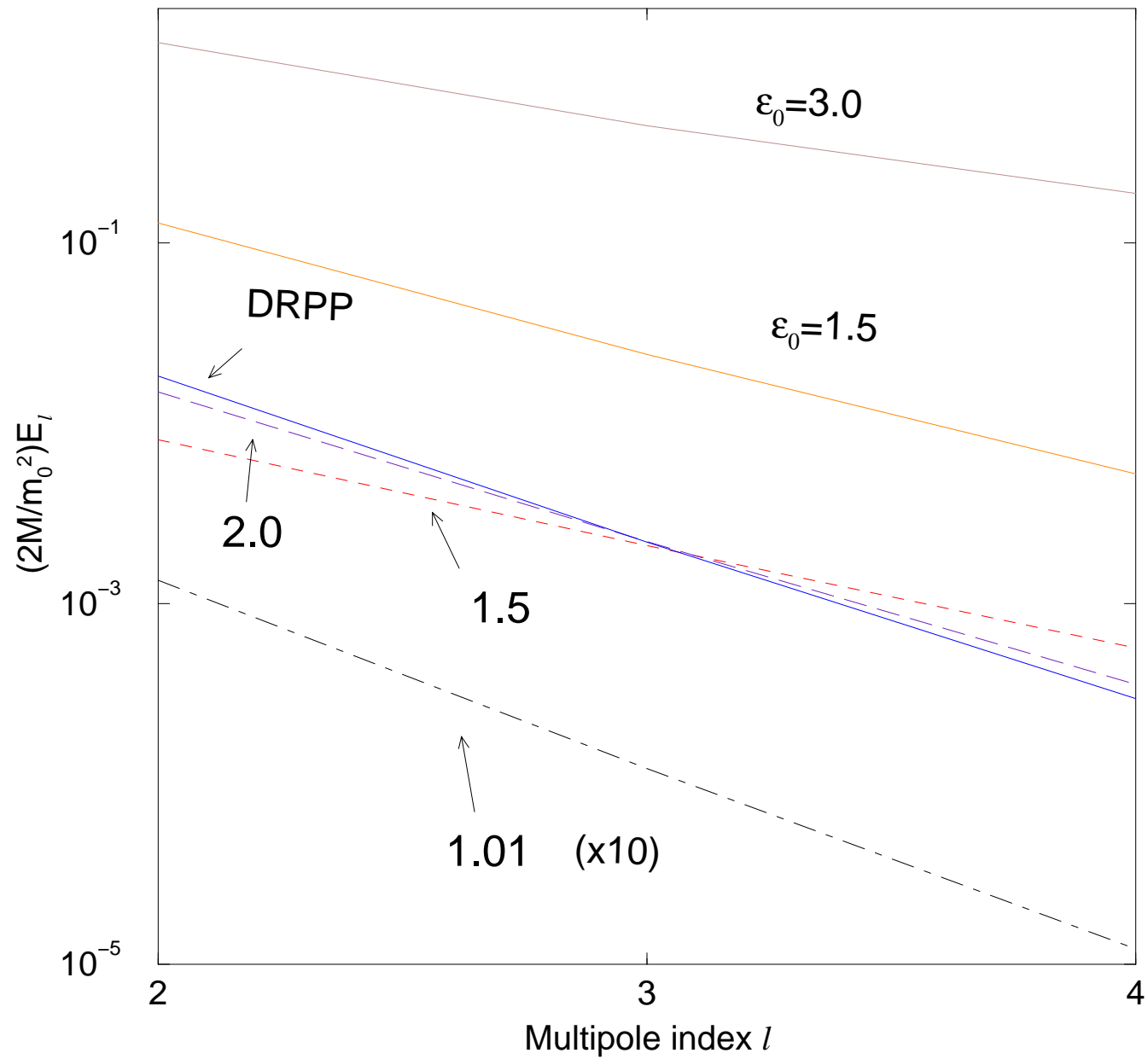


Figure 8

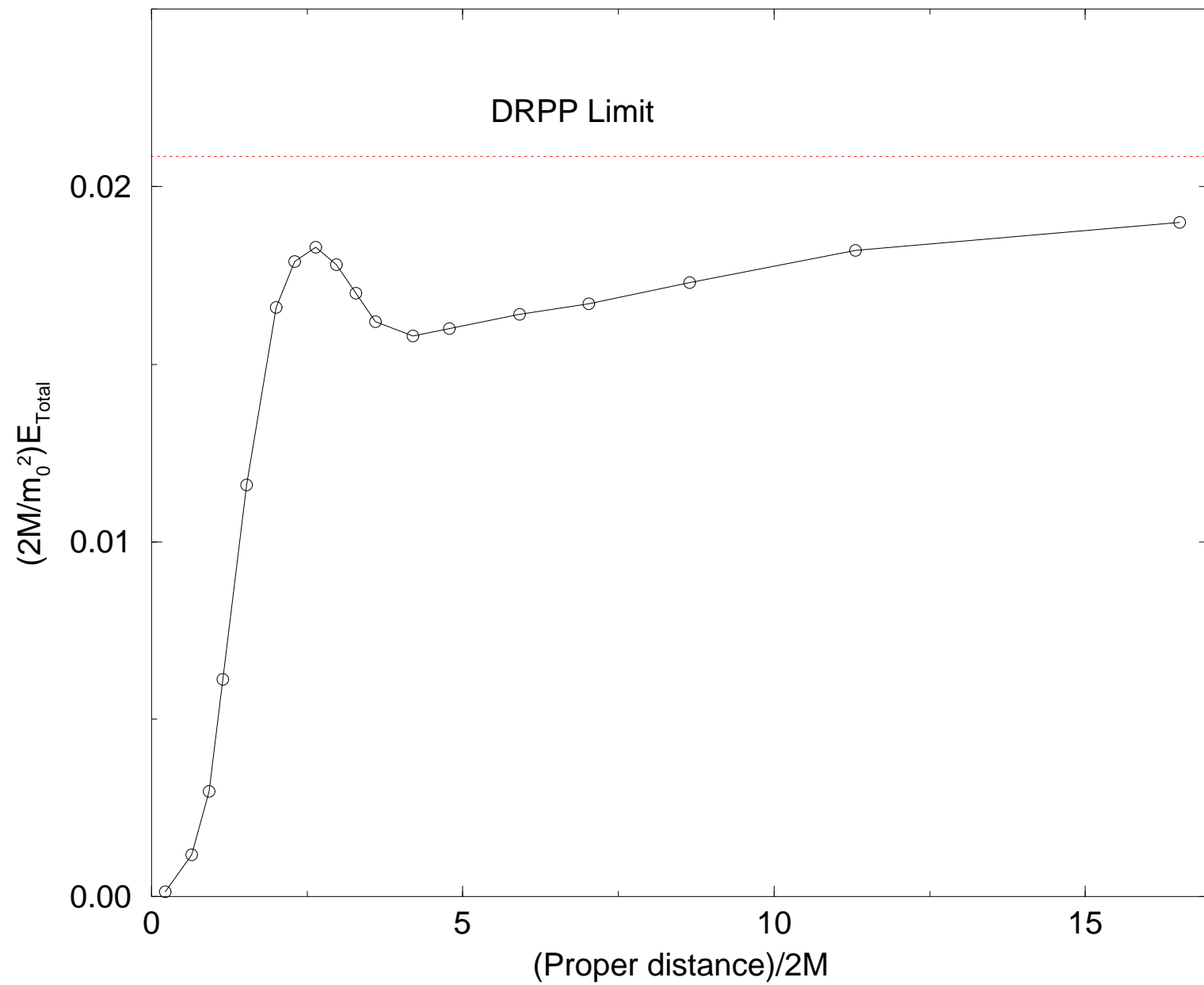


Figure 9a

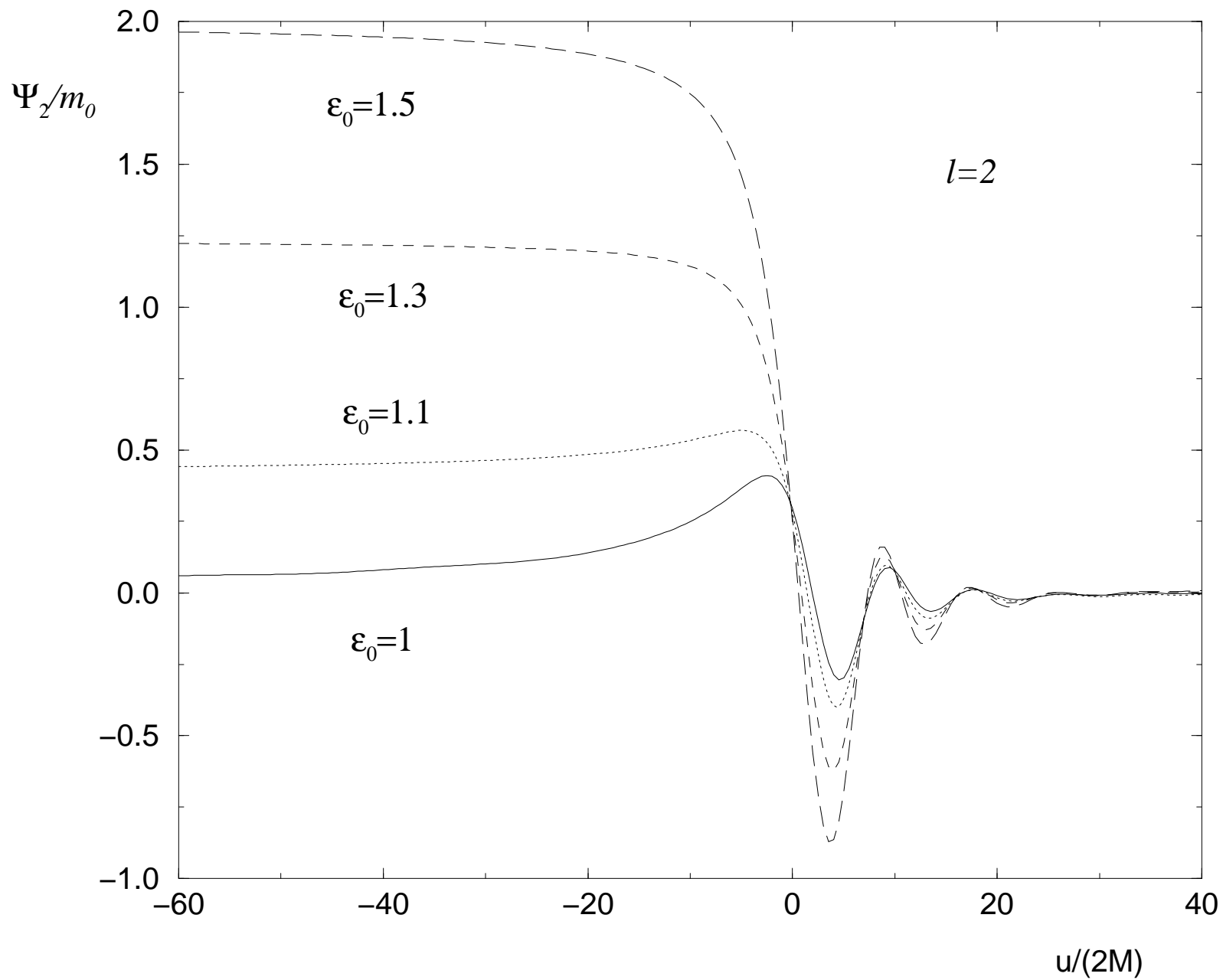


Figure 9b

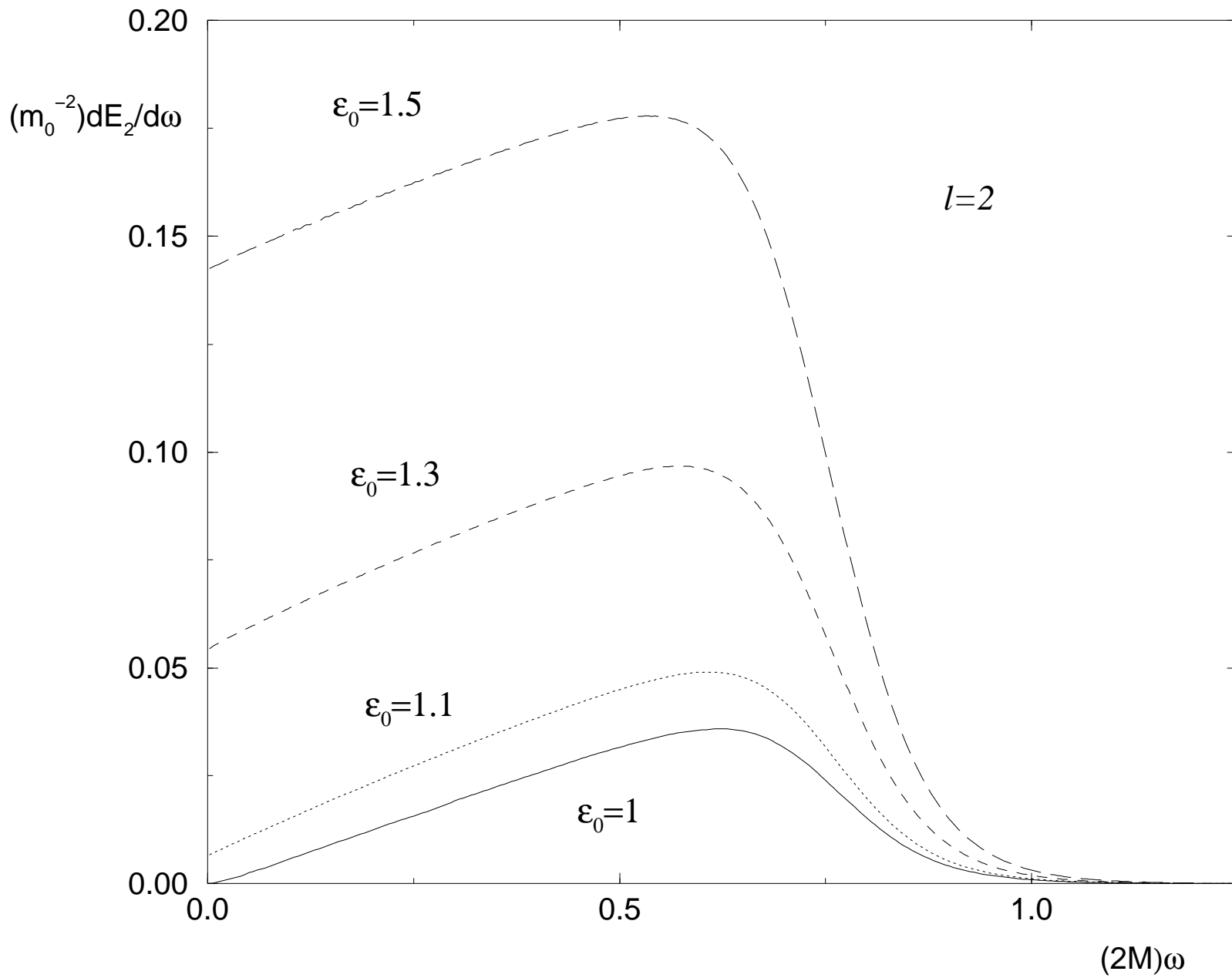


Figure 9c

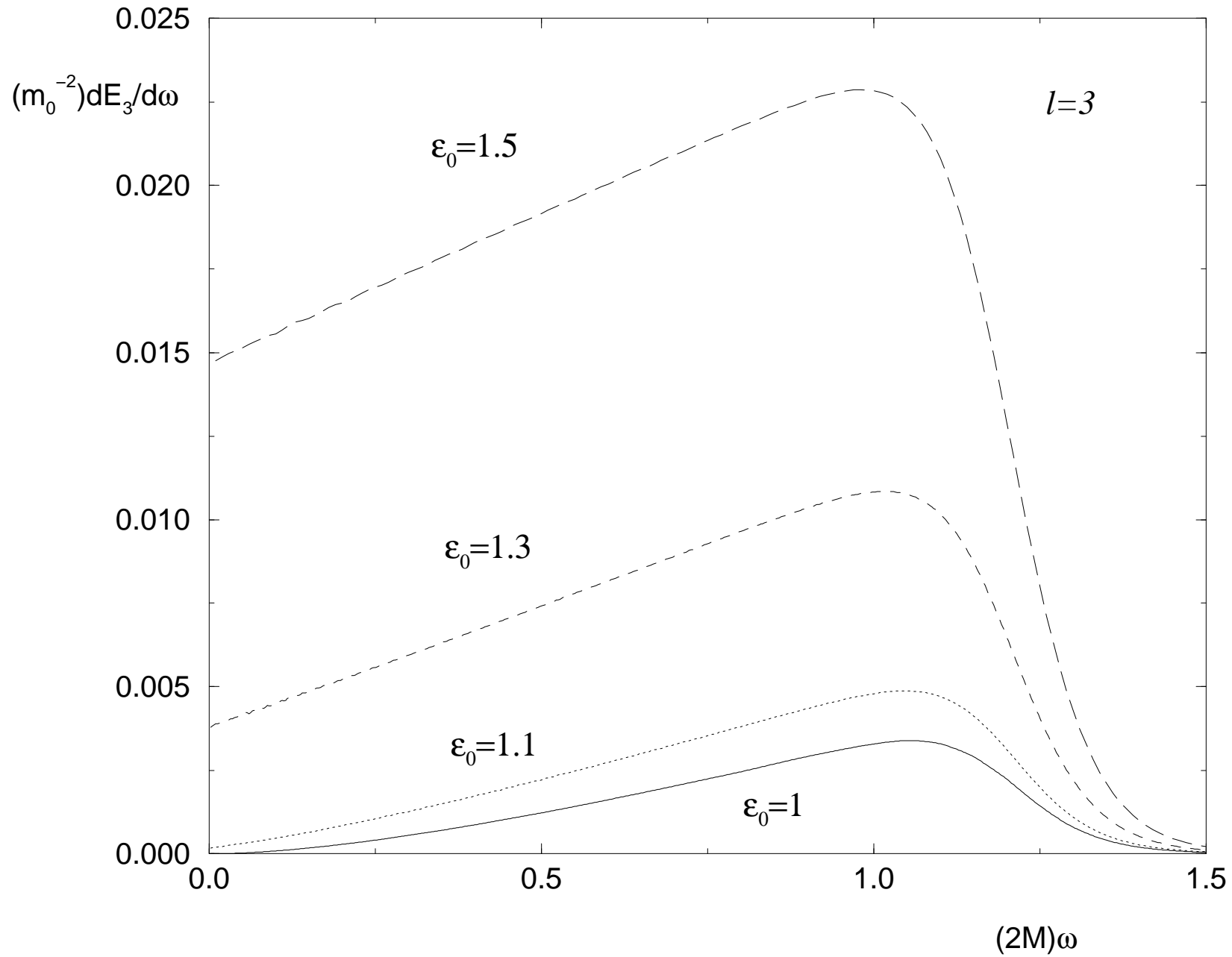


Figure 9d

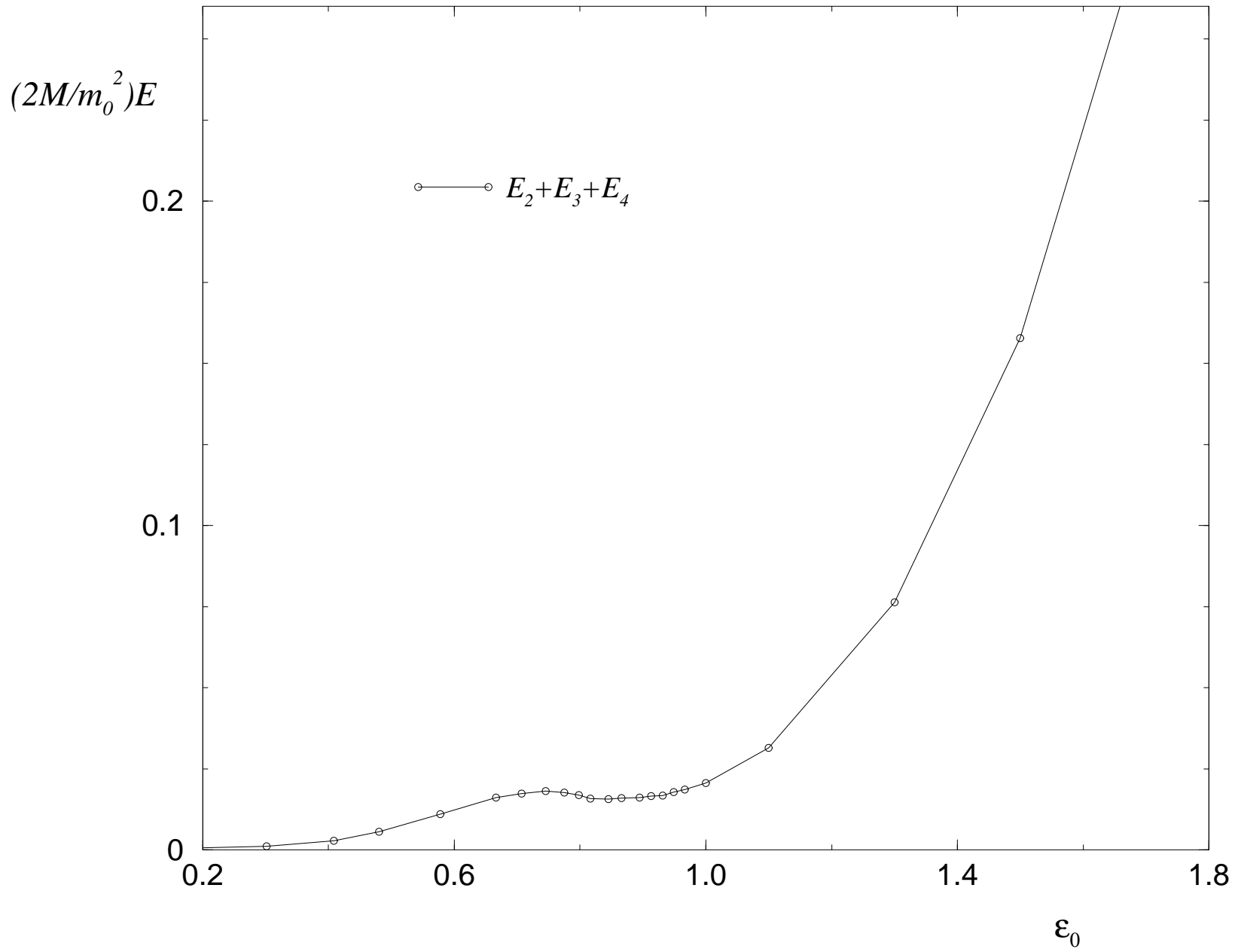


Figure 10

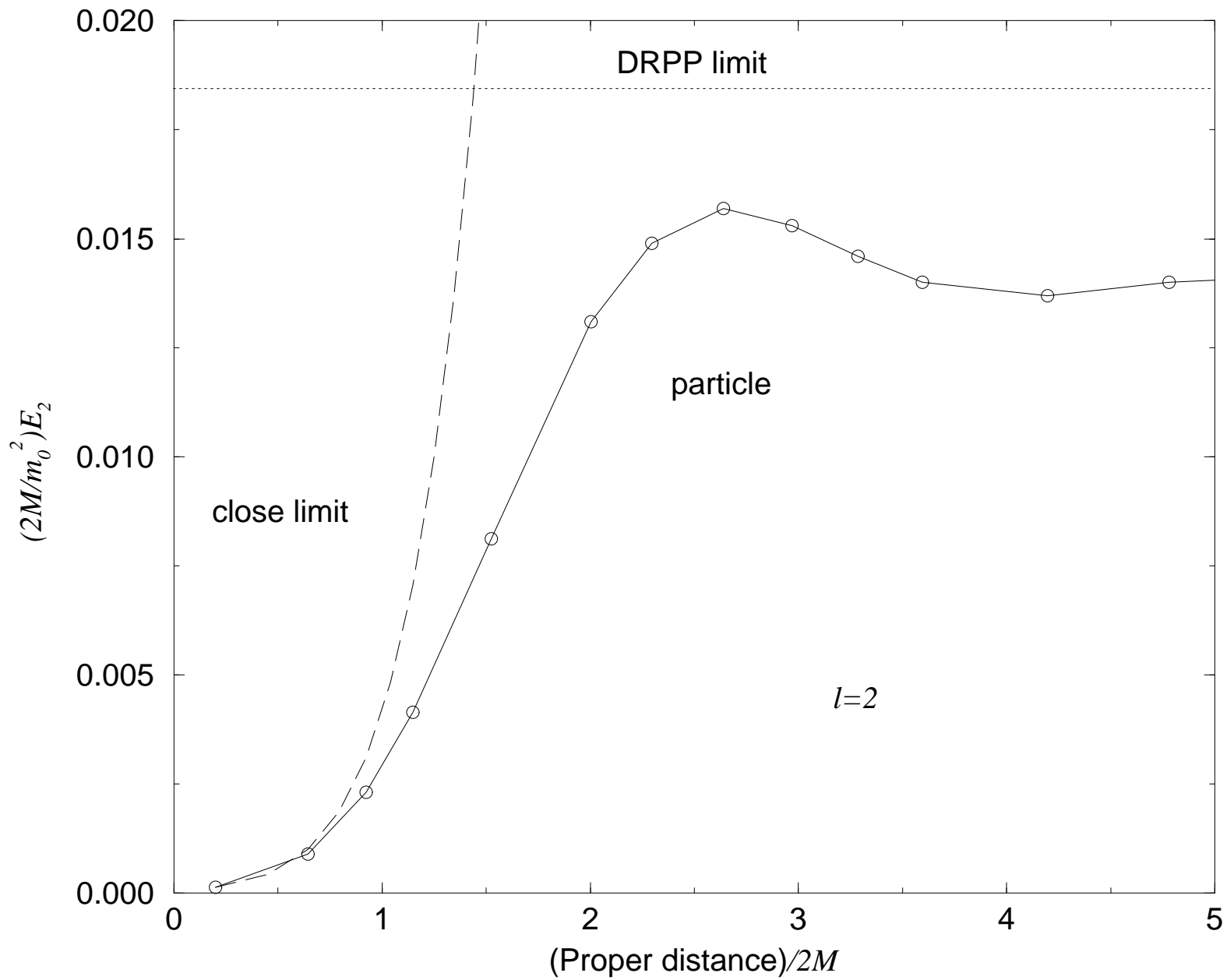


Figure 11

